Simplified Madymo Seated Human Body Model for Motion Comfort Evaluation

by

Junda Wu

to obtain the degree of Master of Science
in Mechanical Engineering
at the Delft University of Technology,
to be defended publicly on Monday August 29, 2022 at 3:00 PM.

Student number:	4960157	
Supervisors:	Dr. ir. R. Happee	TU Delft
	Dr. R.R. Desai	TU Delft

TU Delft

Preface

I have spent four years for Master degrees in TU Delft. With my thesis project, Simplified Madymo Seated Human Body Model, I finally finish my Master of Science degree in Mechanical Engineering. Hereby I would like to express my gratitude to some people.

First of all, I would like to thank my supervisor Professor Riender Happee. I am not good at communicating with people in English. This leads to the difficulty of finding supervisors and thesis topics. Professor Happee gave me a hand and provided me not only the research assignment but also the thesis topic. Till now I can still remember how I was excited at that moment. In the middle of thesis, I can always get assistance from him when I lost direction. He is an easy-going man who can always give me confidence. I am really grateful to him.

Secondly I would like to thank the counsellor, Lourdes Gallastegui Pujana. Due to my HBO diploma, I had to finish the bridging program to be qualified to the Master program. However all lectures and exams in bridging program were in Dutch. Lourdes helped me with the extra exam time and permission of dictionary for exam. She also helped me to pass Momi progress monitor. You can say that without her, I probably quit university.

Thirdly I would like to thank all other supervisors and people who has helped me. Raj Desai, my daily supervisor, he provides me methodologies of modeling. Mojtaba Mirakhorlo, my research assignment supervisor, he helps me with basic knowledge of Madymo. Marko Cvetković guides me how to start with literature research and Georgios Papaionnou helps me with the report. I appreciate their assistance.

Last but not least, I would like to thank my parents for their unconditional support for my study. I also thank my friends and my teammates of DCF (Delft Chinese Football Club). Although four years is long, they are always with me physically and mentally.

Junda Wu
Delft, August 2022

Abstract

People need to have a comfortable experience in vehicles nowadays. However, they are continuously exposed to vibrations from the vehicle. Madymo active human models (AHM) can be used for comfort analysis and to learn how vibrations influence the human body in several aspects. However, existing AHM are very time-consuming due to their complexity, and the correspondence with human comfort data is only reasonable. In order to more effectively analyze motion comfort, a computationally efficient simplified human model (SHM) is developed and validated. The human body model has 36 degrees of freedom (DoF) considering the following segments: pelvis, two thighs, two lower legs, two feet, lower torso, upper torso and head. The model is validated in fore-aft, lateral and vertical vibrations. The model's postural stabilization parameters are tuned manually, by gradient search and grid search in sequence. Manually tuning gives a group of initial values of parameters for further optimization. According to the results, failure of the gradient search illustrates that this optimization problem is non-smooth. At the same time, grid search gives a relatively better result but also shows that the current cost function does not perfectly represent a good fit and needs improvement. A comparison between AHM and the SHM shows that the SHM has a similar or even better fit for most signals while being a largest factor 116 faster. A comparison of parameters between SHM and multibody human models in the literature shows that the structure of models affects the values of the same parameters. A comparison of different time steps illustrates that shorter time step does not necessarily give higher accuracy for this SHM. Suggestions such as adding muscles and changing body shapes are given for further improvement.

Tables of Content

List of Figures

List of Tables

List of Abbreviations

CPU	Center processing unit
DoF	Degree of freedom
FE	Finite element
AHM	Madymo active human model
SHM	Simplified human model
WBV	Whole body vibration
XML	Extensible Markup Language
3D	Three-dimensional
2D	Two-dimensional

1. Introduction

1.1 Background

In future mobility, the motivation to ride a driverless vehicle is not only to commute but also to have leisure time in the vehicle. However, being exposed to whole-body vibration (WBV) produced by the vehicle, occupants may feel discomfort while such vibrations could even cause low back pain and injuries in the lumbar spine. At the same time, symptoms of motion sickness can occur. Therefore, it is important to investigate how vibrations are transmitted through the human body and how the human body responds to WBV. Doing experiments is one way to carry out the study by obtaining real data from experiments. However, experiments cost manpower, and it is possible to cause health discomfort. Doing multiple experiments is not realistic when extra data is needed. For reasons of health issue and data collection, it is efficient to build a seated human body model in a vehicle for comfort research.
Madymo, whose full name is mathematical dynamic modeling, is a software used to simulate occupants with different postures such as erect and slouched for comfort analysis. It has 3 built-in adult occupant models [32], which are a small female model representing the 5th percentile female population, a mid-size male model representing the 50th percentile male population and a large male model representing the 95th percentile male population (see Fig. 2.3). This model are made up of large amount of rigid bodies (multibody) and finite element surfaces capturing the skin for contact interaction. Postural stabilization is captured using line element muscles. Therefore, these existing human models are time-consuming.

1.2 Motivation

In order to reduce run time of vehicle comfort simulation, a SHM should be built as a replacement of complex AHM for specific analysis. The simplified Madymo human body model would allow researchers to have insight of human body response to WBV without consuming large amount of time.
According to Wu [24] and Yu [29], researchers have created three different kinds of biomechanical human body models: lumped masses model, multibody human body model and finite element (FE) model. Lumped masses model is the simplest model in which human body segments are regarded as rigid mass and can only have translational movement in one direction. Due to the simplicity, the lumped model usually does not have a good representation. FE model is made up of a large amount of mass, spring solid and beam elements, and can be used to model detailed structures, i.e. skeletons and muscles and predict human motions. However, due to its high

complexity, it is also time-consuming to be used in simulation. Therefore, the multibody human body model is a compromising model whose development is required to overcome such problems. It requires dimensions of each human body segment and allows translational and rotational movements in any direction. With more degrees of freedom (DoF), the multibody model could have a better representation than the lumped model. Lower complexity makes the multibody model more efficient than the FE model.
The objective of this project is to build a simplified Madymo multibody seated human body model that can be used for analyzing human response in vehicle environment. The SHM would be more computational efficient than complex AHM, delivering similar or even less error than the complex model.

1.3 Thesis Objective

The thesis objective is to develop a simplified Madymo human body model that can replace AHM for human response. Therefore, this SHM should be able to be used in same environment as the complex model. As a SHM, its construction should be simpler than AHM and it should take less time to run it. Therefore the model is designed to be as simple and fast as possible, providing a good fit with available experimental motion data. Here we consider head, trunk and pelvis as these are essential in comfort perception, and consider 3D motion in translation and rotation.

1.4 Approach

The objective of the research is to predict the human body response to vehicle vibration through the SHM. The first step to achieve this goal is building a parametric seated human body model in Madymo. Secondly, parameters are tuned by specific optimization algorithm to fit existing experimental vibration data. Finally, the integral time step and backrest's shape are varied. Results of various configurations in the simplified model are compared with the complex model as well.

2. Development of simplified seated human model

In order to build a simplified Madymo seated human body model, models in literature and AHM are studied. The structure of the SHM will be built up by Madymo elements based on these models. Finally, the environment is set up to simulate the experiment.

2.1 Two existing three-dimensional (3D)seated human body model in literature

A literature research is conducted for multibody human body modeling. There are various multibody human body models in literatures [5,6,11,13,15,16,21,23,24,29]. These models can be divided into two types: two-dimensional (2D) and 3D models. However, 2D models are not sufficient as motion comfort in vehicle results from 3D motion. Two 3D models, representing a seated human body, will be discussed below and their body segments are illustrated. The first model shows the shapes of body segments and the latter mainly illustrates the types of joints.

2.1.1 A 3Dmultibody model without legs and feet

Wu's model [24]is exposed to a vehicle circumstance of combined lateral, vertical and roll vibration. This model is divided into 6 segments: pelvis, lower torso, upper torso, head, left thigh and right thigh. Body segments are both connected by linear translational and rotational springs and dampers. In this model, pelvis, lower torso and upper torso are modeled as cubic blocks while the two thighs are modeled as cylinders, and the head is modeled as an ellipsoid. To represent seat contact, the human model and the seat model are connected by linear translational and rotational springs and dampers. All translational springs and dampers are along lateral and vertical directions and rotational springs and dampers are about fore-aft direction.
Due to the braking of the vehicle, occupant's body is always induced to pitch motions. During these motions, feet can support the human body contributing to pitch motion. Thus, this model could be further improved if lower legs and feet are added and aft-fore vibration is taken into account.

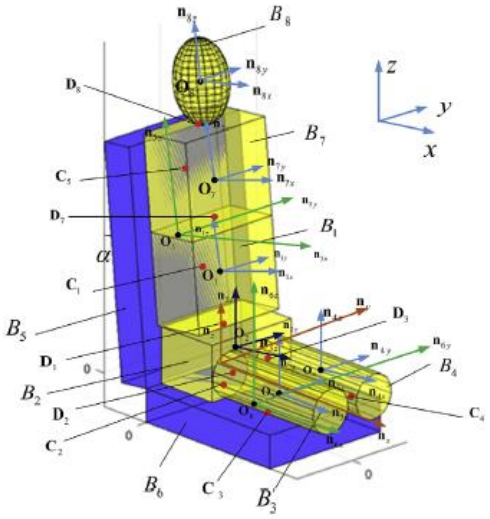

Figure 2.1The seated human model with 16 DoF without legs proposed by Wu [24].

2.1.2 A full seated human model

Mohajer [15] proposed a 3D whole-body model which is made of 15 body segments: pelvis, torso, head, two upper arms, two forearms, two hands, two thighs, two legs and two feet, which is shown in Fig. 2.2. All of these segments are interconnected by revolute joints or spherical joints and none of them are translational. Mohajer proposed two nonlinear models of spring-damper sets to the contact between the human body and seat foam. Same as seat-human contact force, resistance in joints is also considered nonlinear.

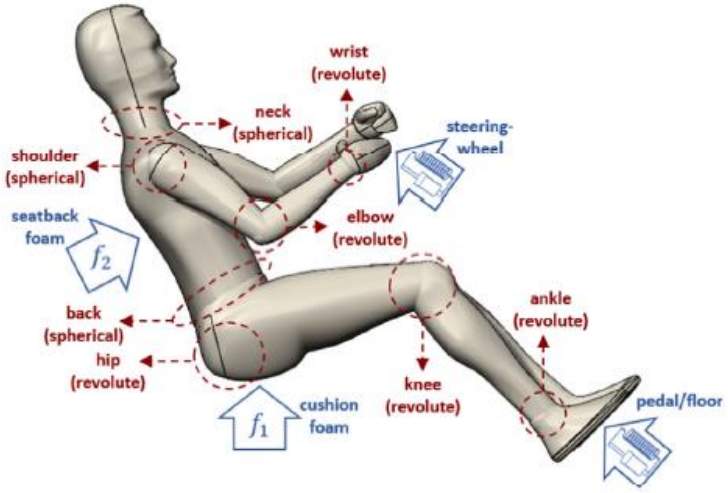

Figure 2.2 A seated humanmodel with 45 DoF and specific joints proposed by Mohajer [15].

2.2 Madymo active human model

Madymo has two active human models, which are available in one baby and one mid size male[32].

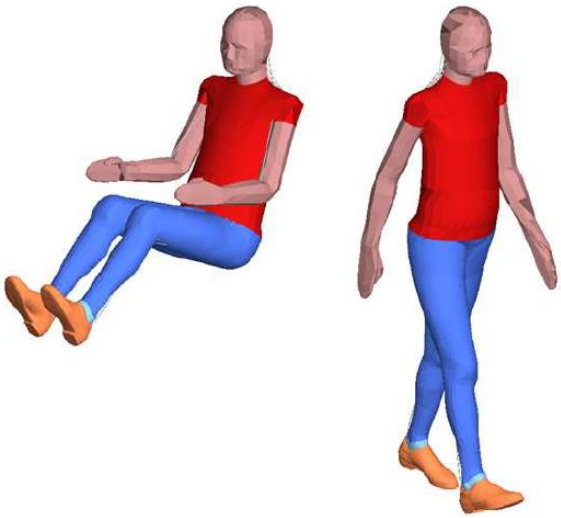

Figure 2.3 Madymo active huma model of mid size male.

Each of these models consists of 190 bodies. The vertebrae are modeled as rigid bodies connected by free joints with nonlinear lumped joint resistance models in the spine and neck. Thorax and abdomen consist of 4 flexible bodies, respectively. Each flexible body is connected to the closest rigid vertebral body of the spine. These flexible bodies allow simulation of rib cage deflection in frontal and lateral impact which is relevant for injury prediction in impact conditions. However, these will not be relevant for comfort evaluation. The upper extremity is allowed to move by the shoulders. The shoulder has joints connecting the humerus, scapula, clavicle and sternum. Limbs of these human body models are modeled as rigid bodies connecting to the branch by spherical joints. Skin is modeled as a mesh of triangular elements (facet surfaces) supported by nearest rigid bodies and flexible bodies. The lower end of the spine is the pelvis bone, which is modeled as rigid body with facets surface. This facet pelvis could be used to contact the environment.

Compared with multibody human body models in literature [24,29], the AHM are more advanced with 3D skin (facets) enabling more realistic interaction. Full multisegment spine reflects more details of torso responses. Advanced postural control also helps the active model to behave more closer to a real human. The shoulder is more complex than only one revolute or spherical joint.

However, the resulting complexity increases the run time, where a 30-second simulation requires about 3 hours when using a simple seat model with ellipsoid seat base and a simple FE seat back model [33]. Here a time step of 5e-5 second is used since higher time step leads to instability in the shoulder or thorax area. Therefore, a simplified model is necessary. This was developed using a generic Madymo solver using elements described below.

2.3 Elements of Madymo multibody models

The Extensible Markup Language (XML) file is the input file of Madymo. It is made up of elements and attributes. The parent element contains children's elements. Therefore, Users define a root element, and all other elements are extended from it.

The human body is made up with different elements. Bodies, surface and joints need to be defined. Necessary elements would be interpreted in the following sub chapters.

2.3.1 Body element

The BODY element defines bodies. The most used BODY element is BODY.RIGID. Each body of Madymo has a coordinate system. Mass, centre of gravity and moment of inertia are attributes under this element.

2.3.2 Surface element

The SURFACE Element defines the surface of a body. There are only three regular surface elements: ellipsoid, cylinder and plane. Surfaces are attached to a body. Users define the position of the surface in the coordinate system of its attached body. The shape of the surface and the characteristic of contact are defined as an attribute under this element. Not only one surface could be attached to a single body, so the irregular surface of a body could consist of multiple regular surfaces.

2.3.3 Joint element

The JOINT element defines joints, which are the connection between two bodies. Without any constraints, a free joint has 6 degrees of freedom: displacement along the x-axis, displacement along the y-axis, displacement along the z-axis, rotation about the x-axis, rotation about the y-axis and rotation about the z-axis. Different joint elements add different constraints. For example, JOINT.REVO, defining the revolute joint, only allows two attached bodies to have relative rotation around one axis. JOINT.PLAN, defining the planar joint, only allows two bodies to have relative displacement along two axes. The positions and orientation of joints are defined under its children element.

2.3.4 Orientation element

The ORIENTATION element defines orientation and it is used for joint positioning and surface positioning. Two vectors or a rotation matrix can define it. It can also be defined via successive rotations around different axes.

2.3.5 Contact element

The CONTACT element defines the contact of two surface groups. Two surface groups are referred to as attributes under this element. The damping coefficient is also an attribute. In Madymo, contact is not rigid but allows penetration. The principle of

contact is applying force between two surfaces. Take ellipsoid-ellipsoid contact as an example; as Figure 2.4 shows, l_1 is the plane tangent to ellipsoid 1 at point 1, and l_2 is the plane tangent to ellipsoid 2 at point 2. Planes l_1 and l_2 are parallel, and the distance between them is denoted as λ. The penetration of two surfaces is defined as the minimum of λ. The value of applied forces is the function of penetration, and their directions are perpendicular to tangent planes, pointing to the respective interior of ellipsoids.

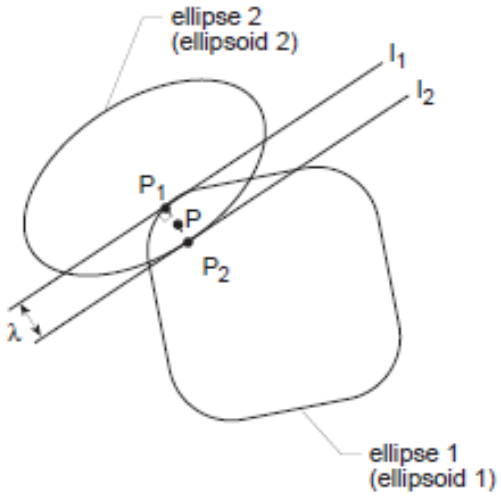

Figure 2.4 Principle of contact between ellipsoids in Madymo

2.3.6 Restraint element

Restraints are force elements defined in the RESTRAINT element. There are different types of restraints: Maxwell restraint, Kevin restraint, point restraint, and Cardan restraint. Maxwell restraint and Kevin restraint connects two bodies by a spring and a damper in a series way and a parallel form, respectively. Point restraint is when two bodies are connected by three perpendicular spring-damper groups (in series). For Cardan restraint, stiffness and damping are applied to rotation about three axes.

2.3.7 Characteristic load element

Users first define a function that describes forces or torque as function of deformation for the restraint. In CHARACTERISTIC.LOAD element, this function is referred to as an attribute. In Madymo, users define a function by defining X-Y pairs. By FUNC_USAGE element, a defined function could be smoother by spline interpolation. In CHARACTERISTIC.LOAD element, user can also define a function that force or torque against deformation rate for damping of restraint, or directly define damping coefficient.

2.4 Structure of the model

Referring to the aforementioned two models in chapter 2.1, a multibody human body model including their advantages, is built. Because facet surface consists of great amount of triangular meshes, using it will cost lot of time to solve. Therefore, only standard multibody surfaces will be used. Standard surface of bodies in Madymo can only be ellipsoid, plane and cylinder. Therefore, “block” shape of human body model like Wu’s model is adapted since Mohajer’s model’s human body shape is complex to be built. Full 6 DoF of each body joint would require the tuning of plenty of parameters. Reducing joint DoF can reduce the model complexity of the model. Therefore, most bodies are interconnected by spherical or revolute joints rather than linear springs and dampers. In order to realistically predict how a seated human body responds to vehicle vibration, legs and feet are also added.

The proposed seated human body model, as illustrated in Fig. 2.6, is made up of 11 segments: pelvis, virtual waist, lower torso, upper torso, head, left thigh, right thigh, left lower leg, right lower leg, left foot and right foot. A simple seat experiment is used to validate the model [33]: Participants are asked to sit in a car mock-up and vibrations of different directions are applying on them. Sensors collect data such as position, velocity and acceleration of body segments. Corresponding to the car mock-up, the Madymo model environment consists of three segments: seat pan, backrest and the floor. The floor is a plane and other segments are ellipsoids. Human body segments are connected by joints. Pelvis and lower torso are connected by a spherical-translational joint, which allows them to have free rotational motion and single-direction (vertical for this joint) translational motion. This vertical motion is essential in capturing the full spinal response in vertical loading. However, Madymo does not have this type of joint. Therefore, a virtual waist is used. The virtual waist is connected with the pelvis by a translational joint and with the lower torso by a spherical joint at the same time. Translational joint is denoted as J_{11} and Rotational joint is denoted as J_{12}. The back spine is modeled as a spherical joint connecting lower torso and upper torso, denoted as J_3. Right hip and left hip are also modeled as spherical joints, connecting the two thighs and the pelvis, which are denoted as J_4 and J_5, respectively. Right knee and left knee are modeled as revolute joints. They only allow thighs and lower legs have relative rotational movement around one axis, which are denoted as J_6 and J_7, respectively. Connecting upper torso and head, neck is modeled as a spherical joint, denoted as J_8. Ankles are modeled as revolute joints, and they connect lower legs and feet, which are denoted as J_9 and J_{10}. The Table 2-1 shows information of joints. Therefore, this SHM model has 36 DoF.

Table 2-1 Joint list of SHM

Number	Joint	Connected body segments		Joint type
J_{11}	Waist	Pelvis	Virtual waist	Translational joint
J_{12}		Virtual waist	Lower torso	Spherical joint
J_3	Back spine	Lower torso	Upper torso	Spherical joint
J_4	Right hip	Pelvis	Right thigh	Spherical joint
J_5	Left hip	Pelvis	Left thigh	Spherical joint
J_6	Right knee	Right thigh	Right lower leg	Revolute joint
J_7	Left knee	Left thigh	Left lower leg	Revolute joint
J_8	Neck	Upper torso	Head	Spherical joint
J_9	Right ankle	Right lower leg	Right foot	Revolute joint
J_{10}	Left ankle	Left lower leg	Left foot	Revolute joint

For the connection between human body and environment, contacts are defined in Madymo. Pelvis, right hip and left hip contact the seat pan. Lower torso and upper torso contact the backrest. Feet contact the floor.

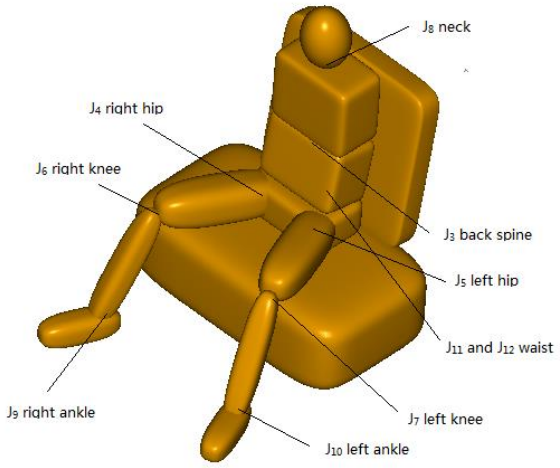

Figure 2.5 Proposed SHM with joints position

2.5 Model data

Pelvis, lower torso, upper torso and feet were initially modeled as cubic block. Thighs and lower legs were modeled as cylinders. However, for better performance of simulating contact, all body segments are modeled as ellipsoids but with different degrees. A mid-size male body size is adopted and its mass is close to the average human model to facilitate comparison. Dimensions of each body segment are referred to Fig. 2.6. Mass of each body segment is also component of the model. These data could be obtained from anthropometry measurements in literature [30]. Moments of inertia are calculated according to models shape of each segment. These model data are listed in Table 2-2.

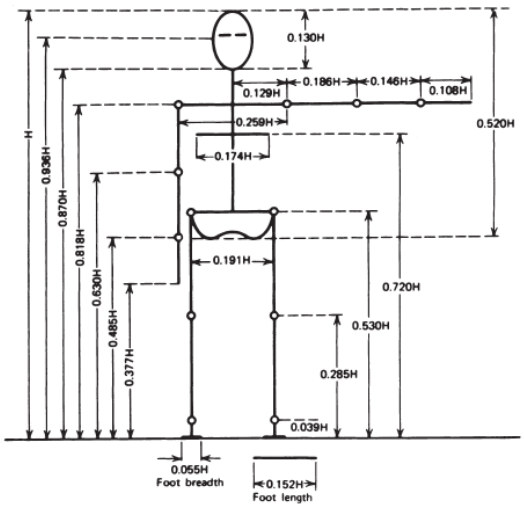

Figure 2.6 Anthropometry measurements of average erect standing male human.

Table 2-2 List of model data

Segments	Ellipsoid Axis Length (times height of human body, which is 1.805m for the current model)			Degree of ellipsoid	Mass (times whole body mass, which is 77kg for the current model)	Moment of Inertia (times value of corresponding segment's mass (kg)) (kg·m^2)		
	x	y	z			I_{xx}	I_{yy}	I_{zz}
Pelvis	0.120	0.191	0.080	4	0.1420	0.003573	0.001733	0.004240
Lower torso	0.100	0.174	0.130	4	0.1390	0.003931	0.002242	0.003356
Upper torso	0.100	0.1740	0.150	4	0.2160	0.004398	0.002708	0.003356
Head	0.100	0.100	0.146	2	0.1000	0.001566	0.001566	0.001000
Thighs	0.245	0.080	0.080	3	0.0465	0.0008000	0.005402	0.005402
Legs	0.246	0.050	0.050	3	0.0810	0.0003125	0.005199	0.005199
Feet	0.152	0.045	0.056	3	0.0145	0.0004300	0.002187	0.002094
Virtual waist	0.000	0.000	0.000	0	1e-10	1e-10	1e-10	1e-10

The joint position is another consideration for the proposed model. The waist joint and back spine joint is placed at the back edge of the torsos and pelvis since the spine locates at the back of a human body. The neck is modeled as a joint connecting the upper torso and head but not a body segment in the model. The neck joint is placed at the centre point of the upper face of the upper torso to have a symmetric structure of the human body. Knees are placed at the end of thighs and legs connecting these two bodies. The middle point of the connection line between two hip joints is consistent with the centre point of the pelvis cube.

In Madymo, each body segment has its own coordinate system. The origin is the gravity of mass center of that body segment by default. Positions of joints which are expressed in different body coordinate system are shown in Table 2-3.

Table 2-3 Coordinate of joints in local coordinate systems (times erect standing height of human body, which is 1.805m for the current model)

Joints	Coordinate system 1	x coordinate	y coordinate	z coordinate	Coordinate system 2	x coordinate	y coordinate	z coordinate
Waist (vertical translation)	pelvis	-0.060	0.000	0.025	Virtual waist	0.000	0.000	0.000
Waist (spherical)	Virtual waist	0.000	0.000	0.000	Lower torso	0.020	0.000	0.065
Back spine	Lower torso	-0.025	0.000	0.065	Upper torso	-0.025	0.000	-0.075
Neck	Upper torso	0.000	0.000	0.075	Head	0.000	0.000	-0.073
Hips	Pelvis	0.000	-0.049	0.000	Thigh	-0.1225	0.000	0.000
Knees	Thigh	0.1225	0.000	0.000	Leg	-0.123	0.000	0.000
Ankles	Leg	0.123	0.000	0.000	Foot	-0.026	0.000	0.000

2.6 The parameters to be identified

Except the predefined human body parameters such as mass and dimensions, remaining unknown parameters should be determined. Each spherical joint has 3 DoF, each revolute joint has 2 DoF and the only one translational joint has 1 DoF. Each DoF is modeled by one linear spring and one linear damper. Therefore, every one DoF corresponds to two parameters. This creates a simplified model of joint stabilization which was also successfully used in other human models for comfort simulation [24,29]. It shall be noted that the stiffness and damping represent passive tissue resistance, as well as postural stabilization using muscle feedback and co-contraction. The active human model separates these contributions using non-linear models. In the SHM, a simpler approach is adopted to reduce Center processing unit (CPU) time and reduce the number of parameters to be considered. This study will illustrate how far such a simplification affects the model accuracy.

The seated SHM has four contact points with the seat (back, pelvis, left thigh and right thigh). In Madymo, the contact force between two ellipsoid surfaces depends on penetration distance, stiffness and damping. For each contact point, two parameters are considered. Table 2-4lists the parameters to be tuned and their abbreviations:

J_9 and J_{10} are ankle joint and knee joint, respectively. C_5 is contact between feet and floor. Variants of parameters corresponding to these two joints and contact points in this SHM do not make obvious influence on the human response after having tuned them. Therefore, they are predefined. Values of relative parameters are referred to the literature [19,29] and are shown in Table 2-5.

Table 2-4 Numbers and abbreviations of parameters

Number of joints or contact points	Parameters	Abbreviations	Units (applied to rest of the report)
J_{12}	Rotational stiffness of waist around x axis	Swx	N·m/rad
	Rotational damping of waist around x axis	Dwx	N·m·s/rad
	Rotational stiffness of waist around y axis	Swy	N·m/rad
	Rotational damping of waist around y axis	Dwy	N·m·s/rad
	Rotational stiffness of waist around z axis	Swz	N·m/rad
	Rotational damping of waist around z axis	Dwz	N·m·s/rad
J_3	Rotational stiffness of back spine around x axis	Strx	N·m/rad
	Rotational damping of back spine around x axis	Dtrx	N·m·s/rad
	Rotational stiffness of back spine around y axis	Stry	N·m/rad
	Rotational damping of back spine around y axis	Dtry	N·m·s/rad
	Rotational stiffness of back spine around z axis	Strz	N·m/rad
	Rotational damping of back spine around z axis	Dtrz	N·m·s/rad
J_4 and J_5	Rotational stiffness of hips around x axis	Shx	N·m/rad
	Rotational damping of hips around x axis	Dhx	N·m·s/rad
	Rotational stiffness of hips around y axis	Shy	N·m/rad
	Rotational damping of hips around y axis	Dhy	N·m·s/rad
	Rotational stiffness of hips around z axis	Shz	N·m/rad
	Rotational damping of hips around z axis	Dhz	N·m·s/rad
J_8	Rotational stiffness of neck around x axis	Snx	N·m/rad
	Rotational damping of neck around x axis	Dnx	N·m·s/rad
	Rotational stiffness of neck around y axis	Sny	N·m/rad
	Rotational damping of neck around y axis	Dny	N·m·s/rad
	Rotational stiffness of neck around z axis	Snz	N·m/rad
	Rotational damping of neck around z axis	Dnz	N·m·s/rad
J_{11}	Translational stiffness of waist along z axis	Swt	N/m
	Translational damping of waist along z axis	Dwt	N·s/m
C_1	Surface stiffness between pelvis and seat pan	Sp	N/m
	Surface damping between pelvis and seat pan	Ds	N·s/m
C_2	Surface stiffness between torso and backrest	Sto	N/m
	Surface damping between torso and backrest	Dsb	N·s/m
C_3 and C_4	Surface stiffness between thighs and seat pan	Sth	N/m
	Surface damping between thighs and seat pan	Dss	N·s/m

Table 2-5 Values of specific predefined parameters

Joints or contact points	Parameter	Value
J_9	Rotational stiffness of ankle around y axis	497N·m/rad
J_{10}	Rotational stiffness of knee around y axis	1500N·m/rad
C_5	Surface stiffness between feet and floor	19843 N/m
	Surface damping between feet and floor	3 N·s/m

The model is assumed to be symmetric about the mid-sagittal plane of human body. Therefore, stiffness and damping of two hips are equalized. The surface stiffness and damping between thighs and seat pan are also equalized.

2.7 Vehicle environment and model positioning

The human body models are settling in a simulating vehicle environment and then response outputs are obtained. In real world, vehicle vibration is combined by vibrations from different directions. In order to study how human body responds to directional vibrations, three directions of vehicle motion are used for validation. Similar with the literature [33], three conditions with erect posture on a simple compliant seat are used: fore-aft, lateral seat and vertical seat motion. The input vibrations are of 0.3 m/s^{2}rms power and their frequency ranges are [0.1 12]Hz. These vibrations in time domain, i.e. seat acceleration, velocity and displacement, are shown in Fig. 2.7-2.15.

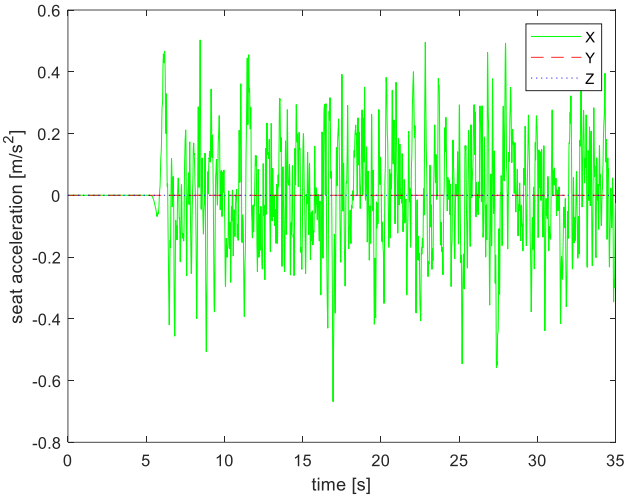

Figure 2.7 Input seat vibration along fore-aft direction between 0 to 40s in acceleration.

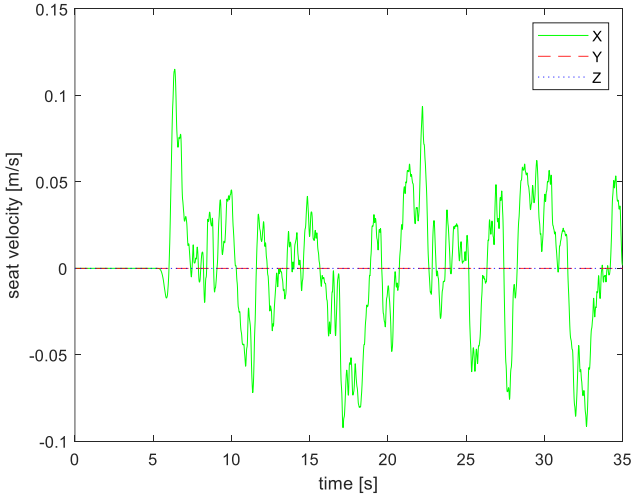

Figure 2.8 Input seat vibration along fore-aft direction between 0 to 40s in velocity.

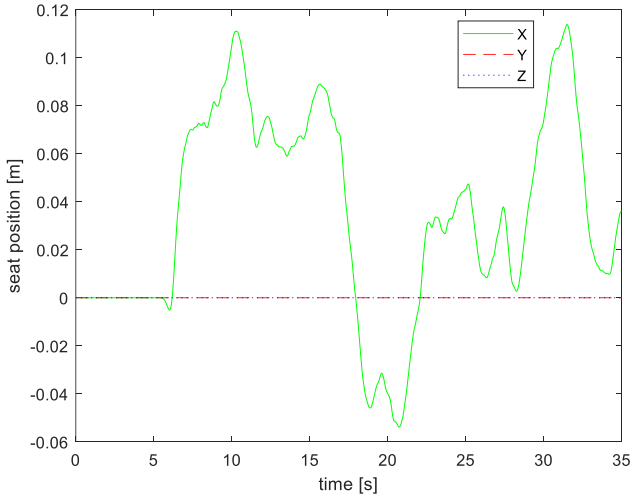

Figure 2.9 Input seat vibration along fore-aft direction between 0 to 40s in displacement.

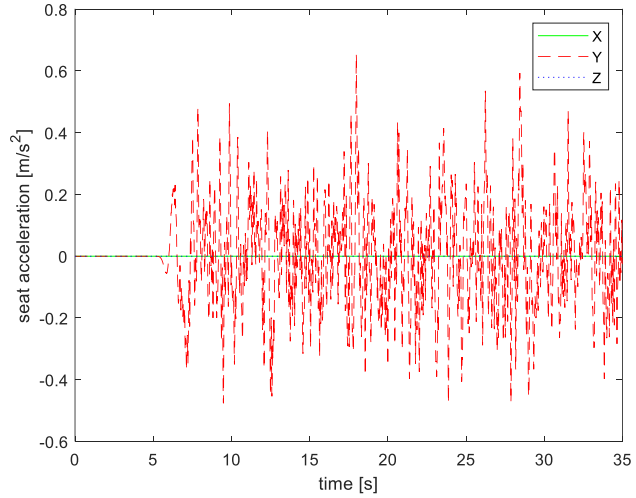

Figure 2.10 Input seat vibration along lateral direction between 0 to 40s in acceleration.

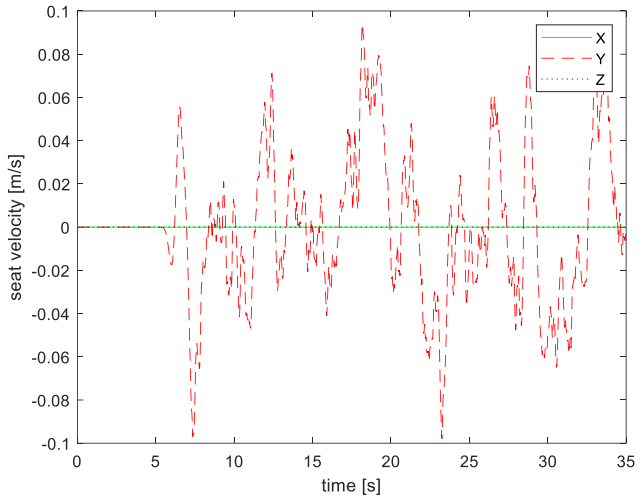

Figure 2.11 Input seat vibration along lateral direction between 0 to 40s in velocity.

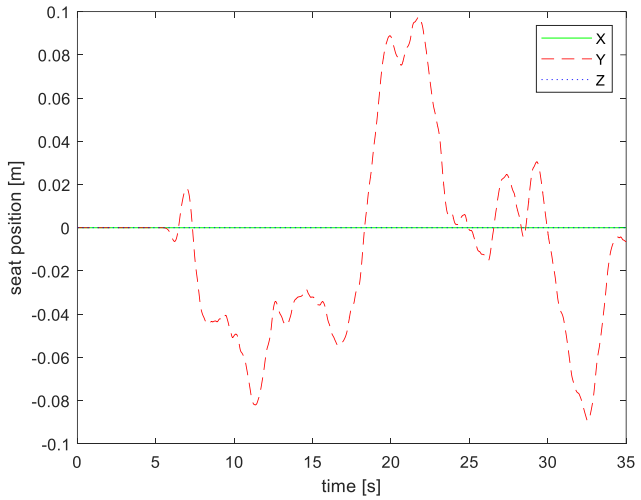

Figure 2.12 Input seat vibration along lateral direction between 0 to 40s in displacement.

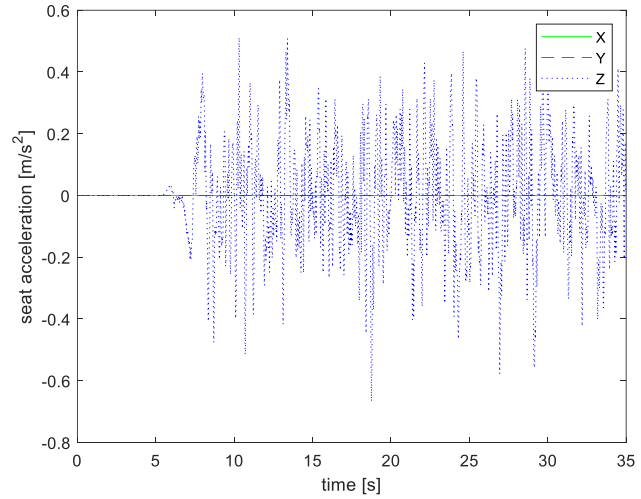

Figure 2.13 Input seat vibration along vertical direction between 0 to 40s in acceleration.

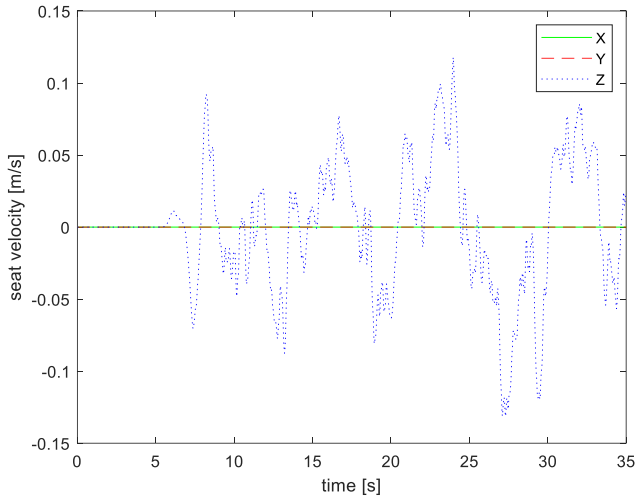

Figure 2.14 Input seat vibration along vertical direction between 0 to 40s in velocity.

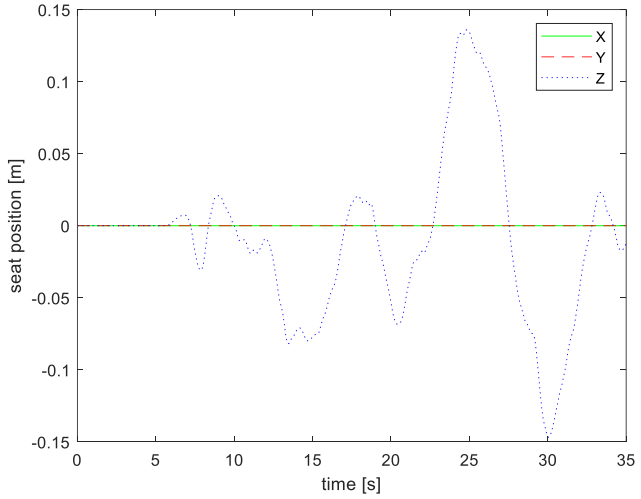

Figure 2.15 Input seat vibration along vertical direction between 0 to 40s in displacement.

The SHM should have same position as AHM on the seat, so that the influence on human response induced by dislocation can be removed. The positioning is achieved by overlapping simplified model on AHM as Fig. 2.16.

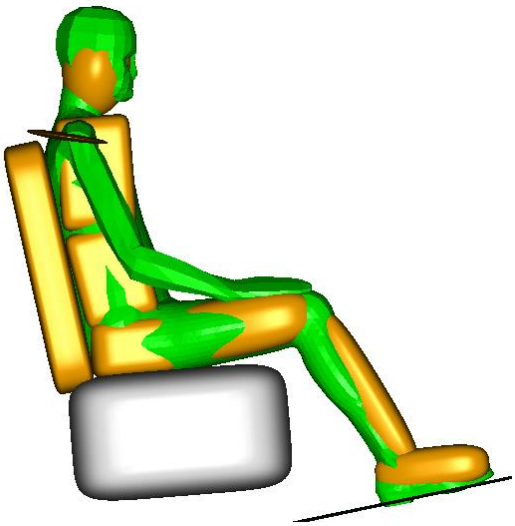

Figure 2.16 AHM (green) and SHM (yellow) are overlapped for initial model positioning.

2.8 Equilibrium settling

At the beginning of the simulation, it is difficult to define a body position and posture leading to equilibrium between the human body model and the seat. Therefore, once the human body is not at the equilibrium point at the beginning, the human body always drops from an unknown height or penetrates in the seat which will cause high-amplitude oscillation due to Madymo characteristic. Such situation makes the SHM unable to simulate an initially seated human accurately, causing the bias in frequency domain. To overcome this equilibrium issue and secure for human body initial positioning, the scenario is simulated for few seconds until it reaches an equilibrium state and then the joint's position information are extracted that time frame.

2.9 Summary

Chapter 2 interprets how seated human body is modeled in literature. Madymo elements of multibody are also introduced. Referring to human body in literature, a SHM with parameters to be tuned is built. The seat with applied vibrations is also built for human models to respond. The model is settling in equilibrium state at last.

3. Method of Parameter Optimization

3.1 Criterion, the cost function for optimization

The SHM is required to have similar response with experimental data. The model should be able to capture the experimental response function in frequency domain. As response functions, specific gains of different body segments will be evaluated.
The gain is defined as:

$$\text{gain} = \frac{\Phi(s_o)}{\Phi(s_i)} \tag{3.1}$$

Wherein s_o is human response of specific body segment in time domain, such as pelvis's vertical displacement or head's pitch. s_i stands for input vibration in time domain. Φ stands for Fourier transform, which means the gain is a function in frequency domain.
The relevant gains should have the minimum errors with respect to experimental data in different seat motions so that the SHM can be the better reference of human response. Therefore, these errors of specific gains are the criterion, i.e. the cost function, for parameter identification. The required body segments for model fitting are head, upper torso and pelvis. Table 3-1 shows all required gains in different seat motions.

Table 3-1 Required gains for model fitting

	Fore-aft seat motion	Lateral seat motion	vertical seat motion
X displacement	√		
Y displacement		√	
Z displacement			√
Roll motion		√	
Pitch motion	√		
Yaw motion		√	

In each seat motion, the gain of experiment as function of frequency is denoted as $G_{ex}(f)$ and the gain of model as function of frequency is denoted as $G_{md}(f)$. In order to put weight on gains of low frequency for fitting, a process of experimental gain is done to conduct a relative gain. The relative gain is denoted as $G_{rel}(f)$, whose expression is:

$$\mathrm{G_{rel}(f)} = |\mathrm{G_{ex}(f)}| + \mathrm{g_{ref}} \cdot \overline{\mathrm{G_{ex}(f)}} \tag{3.2}$$

where g_{ref} is a factor that determines the weighting on lower or higher frequencies with larger g_{ref} to provide weighting on lower frequency. $\overline{G_{ex}(f)}$ is the average value of G_{ex}. The frequency range after Fourier transform, at this step, is [0.3, 100]Hz. The expression of error is:

$$\mathrm{e'_n(f)} = (\mathrm{G_{ex}(f)} - \mathrm{G_{md}(f)})/\mathrm{G_{rel}(f)} \tag{3.3}$$

where n represents different gains. More specifically, n=1,2,3…6 represent x displacement in fore-aft seat motion, y displacement in lateral seat motion, z displacement in vertical seat motion, roll motion in lateral seat motion, pitch motion

in fore-aft seat motion and yaw motion in lateral seat motion, respectively. The frequency domain of e_n is [0.3, 100]Hz at this step. However, lower frequency domain is more interesting. In order to put more weights on low frequency domain, a process is done as follow:

$$e_n(f) = e'_n(f)/\max(f^2, 1) \tag{3.4}$$

Afterwards, high frequency is removed and domain of e_n is defined in (0, 8]Hz.
The criterion of each seat motion is expressed as:

$$e_x = \mathrm{rms}(e_1 + e_5) \tag{3.5}$$

$$e_y = \mathrm{rms}(e_2 + e_4 + e_6) \tag{3.6}$$

$$e_z = \mathrm{rms}(e_3) \tag{3.7}$$

These criterions are the cost function of each seat motion for optimization. Because each parameter almost exclusively affects one seat motion response, the criterions do not need to be summed up. The detail will be interpreted in chapter 4.3.

3.2 Manual Tuning

Initial values of variables are important for optimization algorithm. Proper values of series of variables can help algorithm converge to optimum. Therefore, before using optimization algorithm, a manual tuning is conducted to find proper values of parameters to be tuned.
At the beginning, corresponding parameters in literature are applied to the model and extract the gain plots. The steps of manual tuning are as follows:
1. Each time only one parameter is changed (to increase or to decrease).
2. Record the distinction before and after of that variant.
3. If the error decreases, the current parameters are considered as the best parameters.
4. Repeat step 1 to 3 for each parameter.
5. According to the influences of different parameters, change multiple parameters to attempt to find better results.

Manual tuning stops when it is probably unable to improve the result anymore. The result parameters are shown in Table 3-2.
Time step is a special additional parameter to be decided. It determines the run time of simulation and potentially influence the accuracy of model. Length of time step is set to 1e-3 seconds, which is the longest time step allowing the model to work.

Table 3-2 Outcome parameter's values of manual tuning

Parameters	Values
Swx	10000
Dwx	10
Swy	50000
Dwy	10
Swz	50
Dwz	10

Table 3-2 (continued)

Parameters	Values
Strx	10000
Dtrx	10
Stry	10000
Dtry	10
Strz	20
Dtrz	10
Shx	100
Dhx	20
Shy	2000
Dhy	20
Shz	2000
Snx	8000
Dnx	20
Sny	2000
Dny	2
Snz	50
Dnz	50
Swt	200000
Dwt	5
Sp	80000
Ds	950
Sto	100000
Dsb	800
Sth	1000
Dss	950

3.3 Gradient Search

Since it is a multi-variable problem, it is inefficient to tune all parameter at the same time by the gradient search. In the beginning, for each seat motion, the parameters that potentially make crucial influence on required gains are listed (see Table 3-3).

Table 3-3 Seat motion and corresponding required gains and their essential parameters

Seat motion	Required gains	Parameters tuned in sequence
Vertical seat motion	Z displacement	Swt & Dwt
		Sp & Ds
		Sth & Dss
Fore-aft seat motion	X displacement	Swy & Dwy
	Pitch motion	Stry & Dtry
		Shy & Dhy
		Sny & Dny
		Sto & Dsb

Table 3-3 (continued)

seat motion	Required gains	Parameters tuned in sequence
Lateral seat motion	Y displacement	Swx & Dwx
	Roll motion	Swz & Dwz
	Yaw motion	Strx & Dtrx
		Strz & Dtrz
		Shx & Dhx
		Shz & Dhz
		Snx & Dnx
		Snz & Dnz

Only two parameters are tuned at each step for better optimization efficiency and convergence. These two tuned parameters correspond to one joint or one contact point at the corresponding direction. For example, Swx and Dwy are tuned at the same time because they both correspond to pitch motion of waist joint. After finding minimum when other parameters are maintained unchanged, Stry and Dtry are parameters to be tuned next, and so on. Since vertical seat motion has the least required gains and the least parameters to be tuned, those parameters are tuned first. By the same principle, the second tuning is in fore-aft seat motion and the last is in lateral seat motion. A customized gradient based parameter estimation method was used, incorporating a Gauss Newton scheme with Levenberg Marquardt term to enhance convergence for cases with strong parameter interactions. The maximum number of major iterations is 10 here.

Table 3-4 Initial values and outcome values of gradient search

Parameters	Initial values	Final values of gradient search
Swx	10000	9999.9984
Dwx	10	10.002203
Swy	50000	49999.9554
Dwy	10	9.91234901
Swz	50	49.992981
Dwz	10	9.9992664
Strx	10000	9999.9991
Dtrx	10	9.9965969
Stry	10000	10000
Dtry	10	10
Strz	20	19.996525
Dtrz	10	9.9946786
Shx	100	99.508663
Dhx	20	19.915477
Shy	2000	1997.5683
Dhy	20	19.749846
Shz	2000	1999.9991
Dhz	20	19.999547

Table 3-4 (continued)

Parameters	Initial values	Final values of gradient search
Snx	8000	7999.9999
Dnx	20	20.003109
Sny	2000	2000
Dny	2	2
Snz	50	49.999757
Dnz	50	50.000245
Swt	200000	200000
Dwt	5	4.999954606
Sp	80000	80082.1846
Ds	950	905.640095
Sto	100000	100000
Dsb	800	800
Sth	1000	999.988936
Dss	950	949.994839

The final values and initial values of parameters are listed in Table 3-4. It can be learned that the final value of each parameter only has very small difference with corresponding initial value. The reason could be that this optimization problem is not a smooth problem. A way to illustrate this roughness is to show variants of criterions when parameters are slightly changed by different scales. Fig. 3.1 shows how criterions change (In vertical seat motion, the criterions is relatively too small so they are enlarged by a factor of 10 for better illustration).

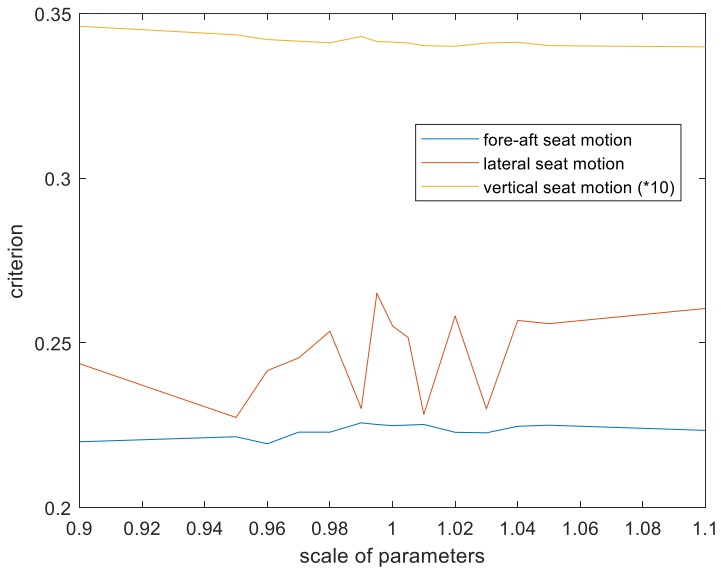

Figure 3.1 Values of criterions vary from different scales of parameters

The Fig. 3.1 shows that the criterion is not monotonous when parameters are slightly changing. Lateral seat motion is apparently not smooth. Therefore, another optimization algorithm is conducted below.

3.4 Grid Search

Grid search would be used to optimize parameters since gradient search does not suitable for this problem. A grid search is to evaluate the criterion value of grid node of parameters. Smaller resolution brings higher probability to find the minimum. Similar to gradient search, two parameters are tuned at one time. The order of tuning is the same as the one in gradient search. The lower bounds, upper bounds and resolutions are shown in Table 3-5. Grid nodes of parameters Sp and Ds and their surface plots are shown in Fig. 3.2. See appendix B for other parameters. The final outcome of grid search is in next section.

Table 3-5 Lower and upper bounds of parameter's value and their corresponding resolution in grid search

Parameters	Lower bound	Upper bound	Resolution
Swt	10000	50000	10000
Dwt	0	200	25
Sp	60000	100000	5000
Ds	0	2000	250
Sth	10000	100000	10000
Dss	0	1250	250
Shy	1000	10000	1000
Dhy	0	75	25
Swy	1000	100000	1000, 10000
Dwy	0	100	25
Stry	1000	100000	1000, 10000
Dtry	0	500	100
Sto	10000	100000	10000
Dsb	0	2000	200
Sny	100	10000	100, 1000
Dny	0	100	50
Shx	1000	100000	1000, 10000
Dhx	0	100	25
Shz	1000	100000	1000, 10000
Dhz	0	100	25
Swx	250	100000	250, 1000, 10000
Dwx	0	200	50
Swz	100	1000	1000
Dwz	0	100	100
Strx	1000	100000	1000, 10000
Dtrx	0	300	100

Table 3-5 (continued)

Parameters	Lower bound	Upper bound	Resolution
Strz	10	1000	10, 100
Dtrz	0	300	100
Snx	100	10000	100, 1000
Dnx	0	100	50
Snz	10	10000	10, 100, 1000
Dnz	0	80	20

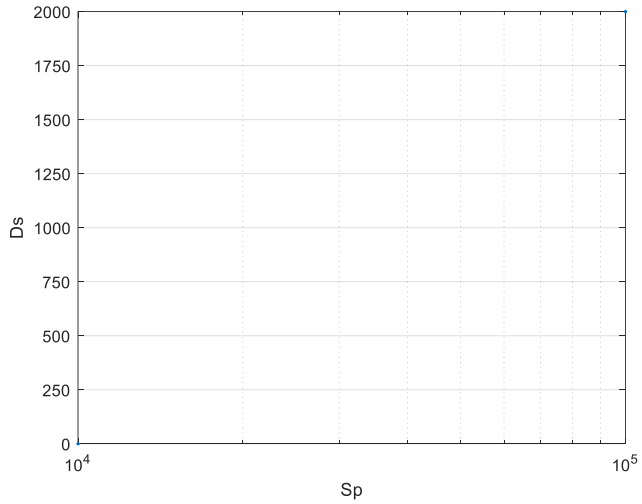

Figure 3.2 Nodes of grid search of Sp and Ds in vertical seat motion

3.5 Summary

In this chapter the process of optimization is discussed to obtain the values of parameters. Cost functions relative to error between model gains and experimental gains in the domain of (0, 8]Hz are created. Manual tuning is done to get better initial values for later optimization. Gradient search is done two parameters by two parameters but the result is obviously infeasible. Grid search is done afterwards.

4. Intermediate result and improvements

4.1 Result of grid search

Outcome parameters of grid search are shown in Table 4-1. The result plot will be shown in chapter 4.3.

Table 4-1 Outcome parameter's values of grid search with initial values

Parameters	Initial values	Outcome values	Lower bound	Upper bound
Swx	10000	500	250	100000
Dwx	10	0	0	200
Swy	50000	80000	1000	100000
Dwy	10	0	0	100
Swz	50	50	100	1000
Dwz	10	10	0	100
Strx	10000	40000	1000	100000
Dtrx	10	0	0	300
Stry	10000	3000	1000	100000
Dtry	10	0	0	500
Strz	20	60	10	1000
Dtrz	10	300	0	300
Shx	100	60000	1000	100000
Dhx	20	50	0	100
Shy	2000	2000	1000	10000
Dhy	20	0	0	75
Shz	2000	2000	1000	100000
Dhz	20	20	0	100
Snx	8000	8000	100	10000
Dnx	20	20	0	100
Sny	2000	9000	100	10000
Dny	2	50	0	100
Snz	50	1000	10	10000
Dnz	50	40	0	80
Swt	200000	50000	10000	50000
Dwt	5	0	0	200
Sp	80000	95000	60000	100000
Ds	950	750	0	2000
Sto	100000	40000	10000	100000
Dsb	800	1600	0	2000
Sth	1000	10000	10000	100000
Dss	950	1000	0	1250

From surface plots of all grid evaluations, it can be learned that optimization problem of Sp and Ds is smooth (Fig. 4.1). The criterion converges to the upper bound of Sp.

Optimization problem of Swt and Dwt is also smooth (Fig. 4.2), whose criterion converges to the lower bound of Swt. However, surface plots of all other grid evaluations are very rough (See Appendix B). Many local minimums locate at many grid nodes.

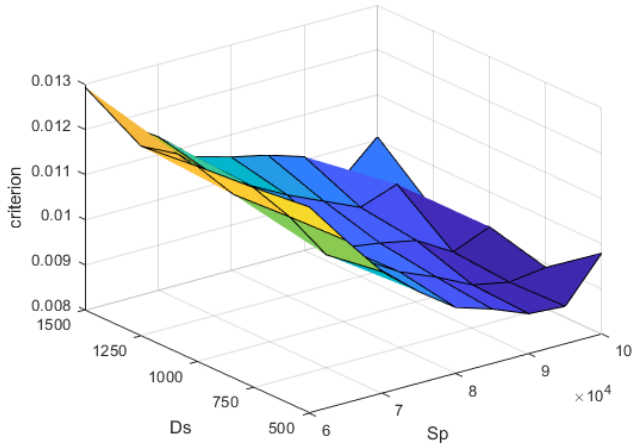

Figure 4.1 Nodes of grid search and result surface plot of criterions for parameters Sp and Ds in vertical seat motion

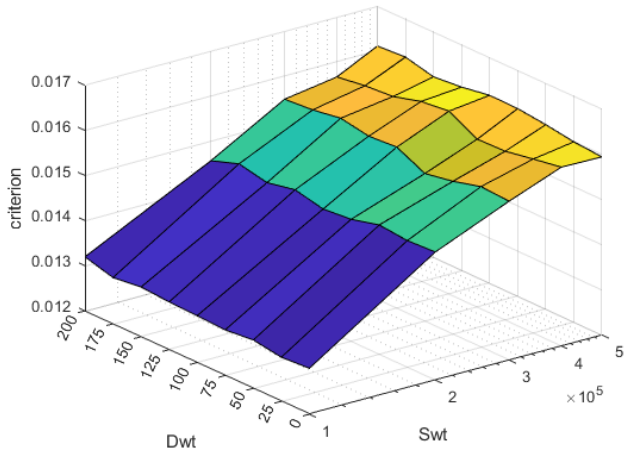

Figure 4.2 Nodes of grid search and result surface plot of criterions for parameters Swt and Dwt in vertical seat motion

4.2 Factors that potentially affect the result

Coherence is an indicator to show if the input and output of model (system) is linearly relative. Higher coherence indicates means higher relevance between input and output. However, some factors such as nonlinearity influence the coherences. Some other factors might influence the reality of the model. Three factors will be interpreted in following sub chapters. Variants of these factors will be applied and chapter 4.3 will show the plots.

4.2.1 Friction at the backrest

The friction coefficient is set to 0.8 on the backrest. Due to the friction on the backrest, the torso of model will have relative movement to the backrest only when the applied force is larger than maximum static friction. After this impending motion, the torso is applying dynamic friction, which causes the friction slip. Such friction slip might cause the nonlinearity that reduces the coherence. Therefore, the friction at the backrest will be removed to compare with the original SHM.

4.2.2 Length of time step

In the above tuning procedure, the length of time step is set to 1e-3 second by default because it is the longest length of time step enabling the model to work, proving faster simulation time. However, shorter length of time step seems to give more realistic result, which are more fitted with the experimentally data. A shorter length of time step, 5e-4, will be used for simulation to compare with the original SHM. Shorter time step will be applied if model of 5e-4 has better fit.

4.2.3 Shape of backrest

The backrest of original model is a big ellipsoid with high degree. It represents a general backrest that allows the human body to fully lean on it. However, in the experiment that produces those experimental data, the backrest is two blocks supporting the human subject to keep the erect posture. In order to have a better fit with the experimental data, the backrest will be modified to the same shape as in the experiment. The result of this special backrest will be compared with the original SHM.

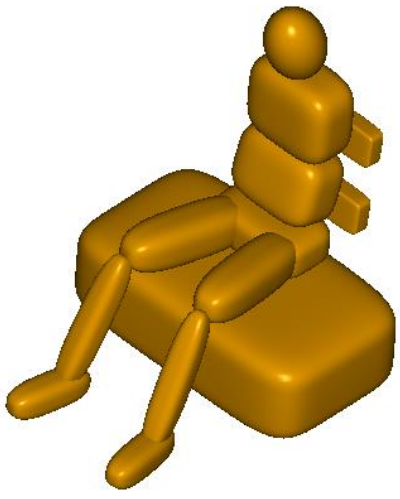

Figure 4.3 SHM with different shape of backrest, which is made of two cubic blocks

4.3 Result plots

Fig.4.3 show the result plots of different varied factors: friction at the backrest, length of time step and shape of backrest. In additional to the gains of required responses, the corresponding coherences are also presented. These results are based on parameters obtained from the grid search.

4.3.1 Result of fore-aft seat motion

According to Fig. 4.4, the overall SHM has a better fitting than AHM in x gains but worse fitting in pitch gains.
For x gains of head and trunk, all SHM basically capture the peak response and match well below 6Hz. However, for x gain of pelvis, all models match well below 2Hz. None of them capture the pelvis peak response. For x coherence, two-backrest model has highest coherence, which is even higher than the experimental x coherence of head.
Complex model fits well in pitch gain of head and trunk below 6Hz since all SHM have much lower gains in this low frequency domain. Only pitch gain of pelvis and trunk of SHM can capture the capture the peak responses. Same as x coherence, two-backrest model has highest pitch coherence, but other SHM have much lower coherences.

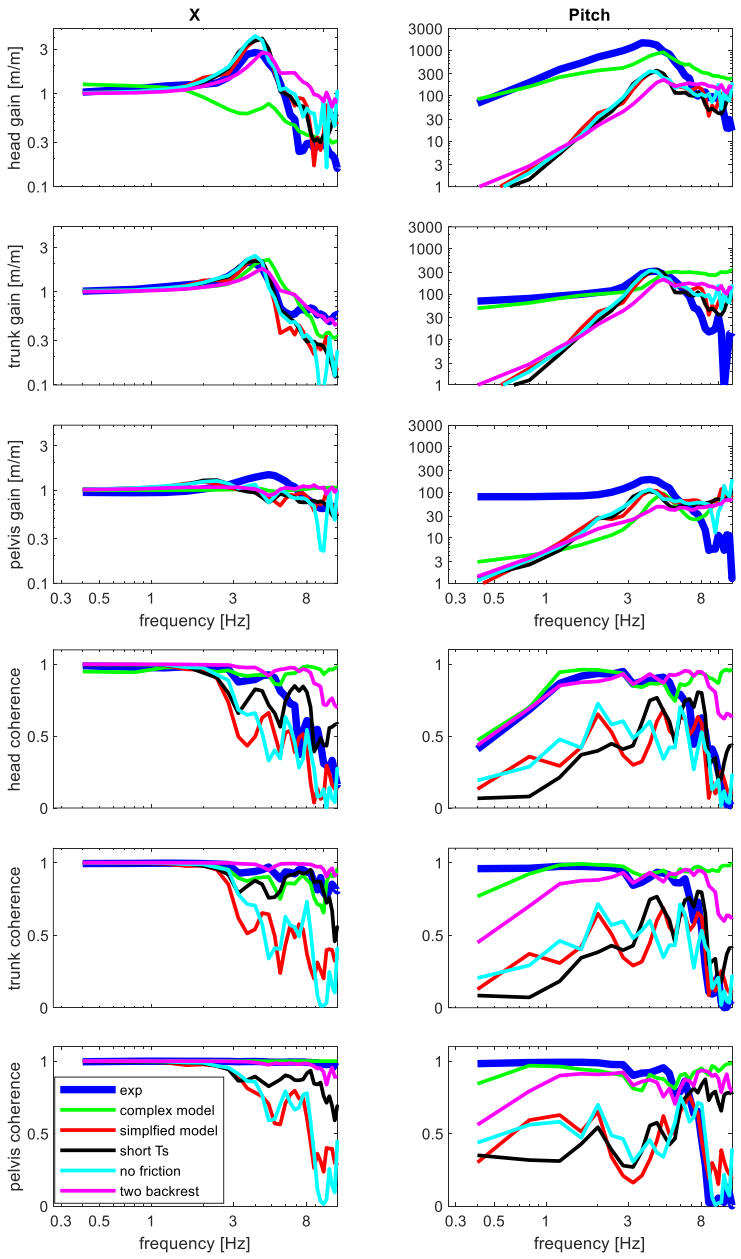

Figure 4.4 Plots of fore-aft seat motion validation with different factors. Gains (upper 3 rows) and coherence (lower 3 rows) for head, trunk and pelvis in x displacement (left column) and pitch motion (right column).

4.3.2 Result of lateral seat motion

According to Fig 4.5, all SHM have similar matching with AHM in all gains except y gain of trunk and roll gain of pelvis. SHM are also fitting worse in these two gains. The AHM model has highest coherence while all SHM have lower coherence.

All models match well in y gain of head below 4Hz expect no-friction SHM. Peak gain of no-friction SHM is a bit higher than experiment. For y gain of pelvis, all SHM match well but becomes their gains become shaper above 5 Hz. Only advantage of

SHM in y displacement is that two-backrest SHM has similar y coherence of head with experiment.

All models have lower roll gains in frequency domain than experiment data. Pelvis roll gains of SHM are much less than experiments.

For yaw gains of head and trunk, all models except no-friction SHM have similar trend with experiment. Yaw gain of head and trunk of two-backrest SHM is lower than other models

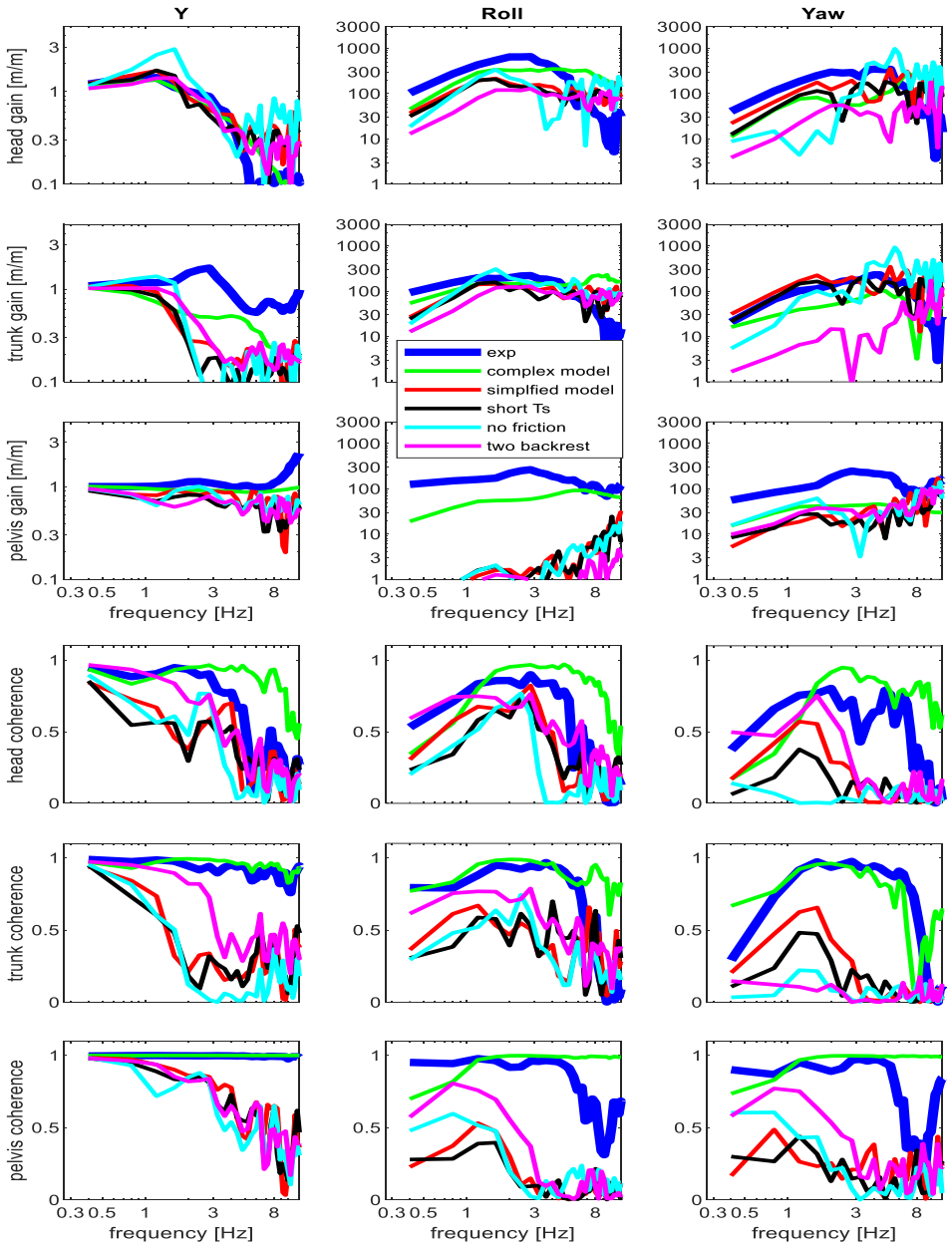

Figure 4.5 Plots of lateral seat motion validation with different factors. Gains (upper 3 rows) and coherence (lower 3 rows) for head, trunk and pelvis in y displacement (left column), roll motion (middle column) and pitch motion (right column).

4.3 Result of vertical seat motion

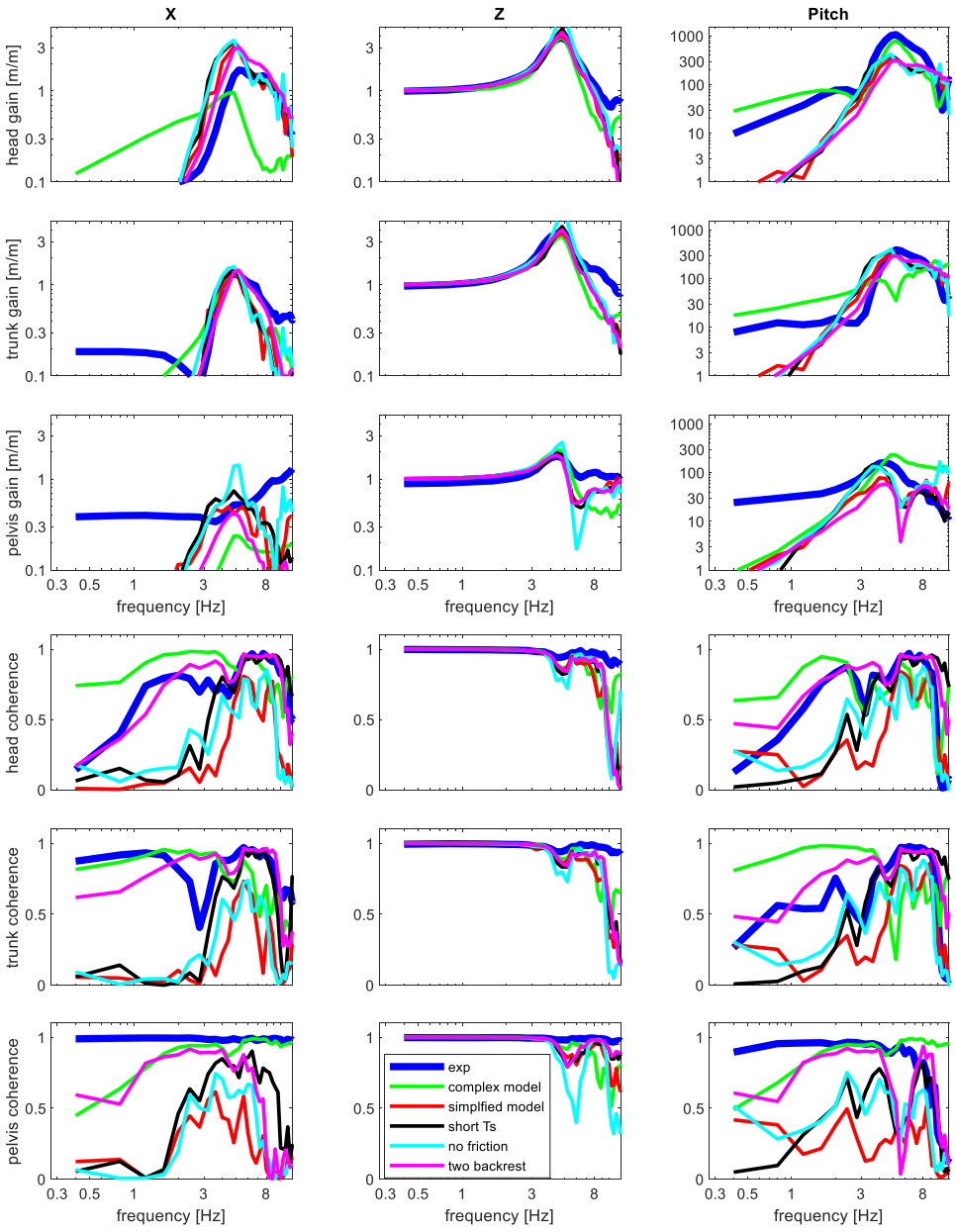

Figure 4.6 Plots of vertical seat motion validation with different factors. Gains (upper 3 rows) and coherence (lower 3 rows) for head, trunk and pelvis in x displacement (left column), z displacement (middle column) and pitch motion (right column).

According to Fig 4.6, all models match well in z gain. They capture the peak gain but z gains of no-friction model are a bit higher. All models have a small valley in z coherence at about 5Hz while z coherence of no-friction model starts to decrease at 5Hz.

4.4 Discussion on intermediate results and potential improvements

According to the overall results, there are no big differences among SHM in gains. The trends in gains of all SHM are basically the same. In low frequency domain below 2Hz, the SHM can predict the gains of human response which has consistent direction with vibrations. In high frequency domain above 2Hz, the SHM can predict the z gains in vertical seat motion of all body segments very well. This is mainly due to the suitable parameters values of seat stiffness and damping and waist's vertical stiffness and damping. In fore-aft seat motion, the SHM has bad fit on pelvis's x gain above 3Hz. This could be caused by high friction on seat pan. High friction makes pelvis doing fore-aft motion.

The no-friction (on backrest) model has larger mismatching to the experiment in gains. In lateral and vertical seat motion, its translational gains are always highest among SHM. Without friction, the torso can easier to do the translational movements, leading to high gains. Same principle also applies to rotational movement in lateral seat motion. Without frictional torque, the body segments can easily rotation. That is the reason of high gain in roll and yaw motion. The no-friction model also has relative low coherence among SHM. That could be concluded that the friction is not the main factor that causes nonlinearity in this model.

Two-backrest model always has highest coherences among all SHM for all human response. The reason could be that two backrests strengthen the power transmissibility from vibrations with respect to one backrest. Moreover, Two-backrest is applied to the experiment [33] obtaining the data, which means two-backrest model is more realistic. Therefore, the new model should use the two backrests.

Shorter-Ts model sometimes also has higher coherence, such as x gains. Since shortening length of time step improves the model to some extent, it is worthwhile to explore if much shorter length of time step would help improve the model prediction. In the new model, different values of time step, 1e-3, 5e-4 and 2e-4, will be compared to each other in the following section.

The back surface of a human body should be continuous. However, this SHM is depressed at the back because torso of model is made up with two ellipsoids with high degrees. A back with smooth surface could potentially help improve the model (Fig 4.7).

In summary, the new model is continuous at the back and lean on the two backrests, which is shown in Fig. 4.8. In the next section these new models will test if the bad prediction of pitch motion in fore-aft seat motion, and trunk's y and pelvis's roll and yaw motion in lateral seat motion, could be improved.

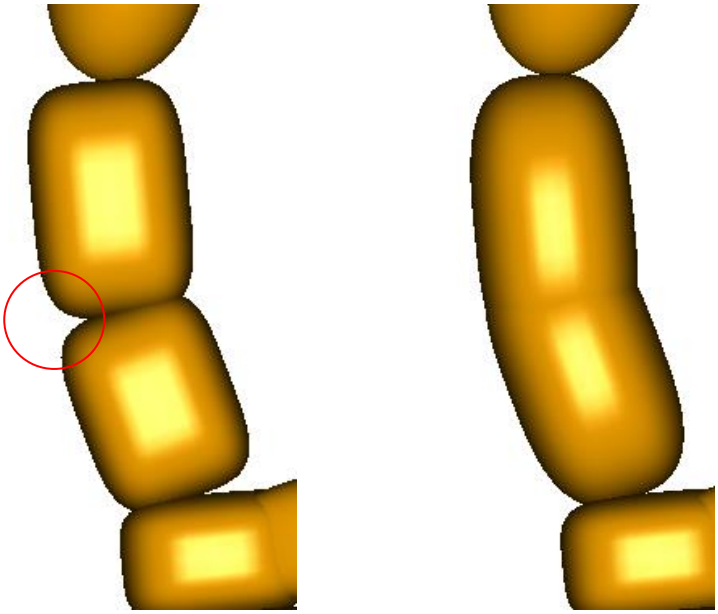

Figure 4.7 Initial SHM (left) with depressed back (in red circle) and improved SHM (right)

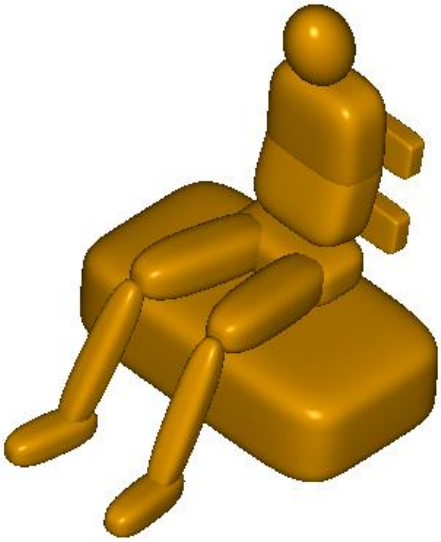

Figure 4.8 An improved SHM body model with continuous back leaning on the two-block backrest

5. Final Result

In this section, resultant of final model in chapter 4.4 with different time step is shown.

5.1 Final result of fore-aft seat motion

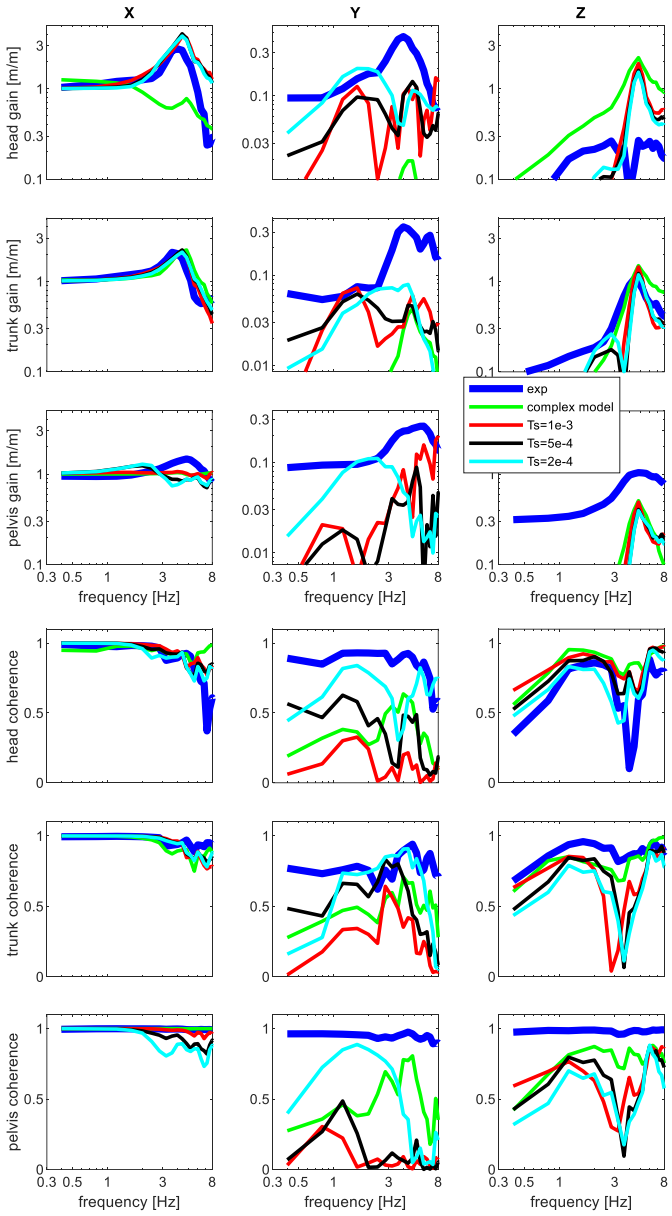

Figure 5.1 Plots of fore-aft seat motion validation with different time steps. Gains (upper 3 rows) and coherence (lower 3 rows) for head, trunk and pelvis in x displacement (left column), y displacement (middle column) and z displacement (right column).

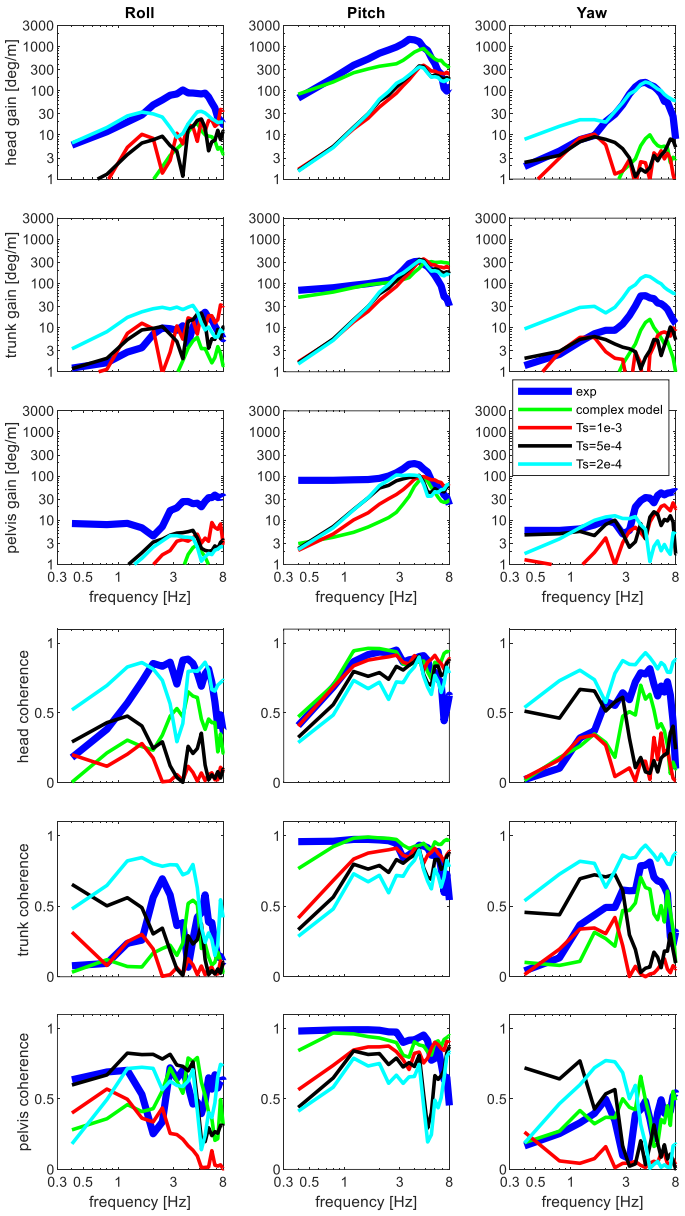

Figure 5.2 Plots of fore-aft seat motion validation with different time steps. Gains (upper 3 rows) and coherence (lower 3 rows) for head, trunk and pelvis in roll motion (left column), pitch motion (middle column) and yaw motion (right column).

Fig 5.1 and Fig. 5.2 shows resultant plot of fore-aft seat motion. The required responses are gains of x displacement and pitch motion. Obviously, the SHM has a better fitting than AHM in x gains but worse fitting in pitch gains.

For x gains of head and trunk, models of all time steps basically capture the peak response. However, for x gain of pelvis, all models only have good fit well below 2Hz. All SHM have much less pitch gains in low frequency domain. Only pitch gain of pelvis and trunk of SHM can capture the capture the peak responses. All models have high x coherence. Among SHM, the Ts=1e-3s model has best fit with experimental data in pitch coherence of head. All SHM have lower coherence in pitch of trunk and pelvis, but 1e-3 model still has highest coherence among SHM.

As to non-required gains, it can be learned that 2e-4 has best fit in yaw gain of head. Although does not fit well, this model also has gains closest to experimental data in y displacement. In coherence of y displacement, roll motion and yaw motion, the order of height is (from low to high) 2e-4, 5e-4 and 1e-3. This law is applied except roll coherence of pelvis.

5.2 Final result of lateral seat motion

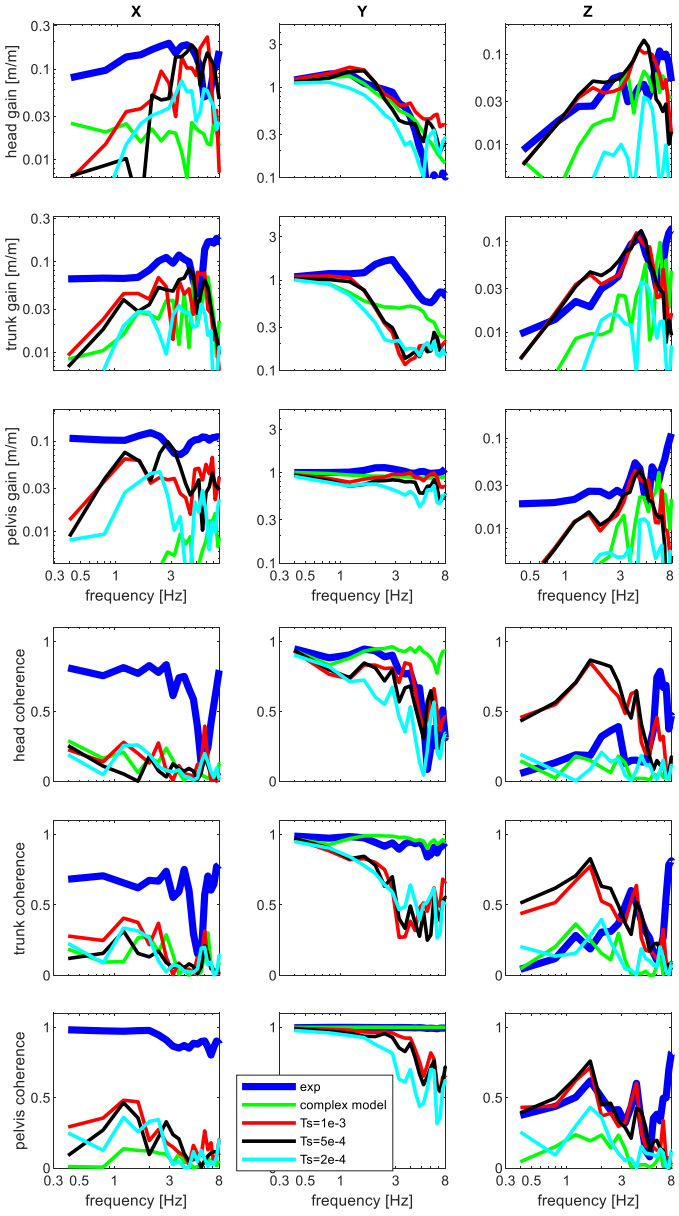

Figure 5.3 Plots of lateral seat motion validation with different time steps. Gains (upper 3 rows) and coherence (lower 3 rows) for head, trunk and pelvis in x displacement (left column), y displacement (middle column) and z displacement (right column).

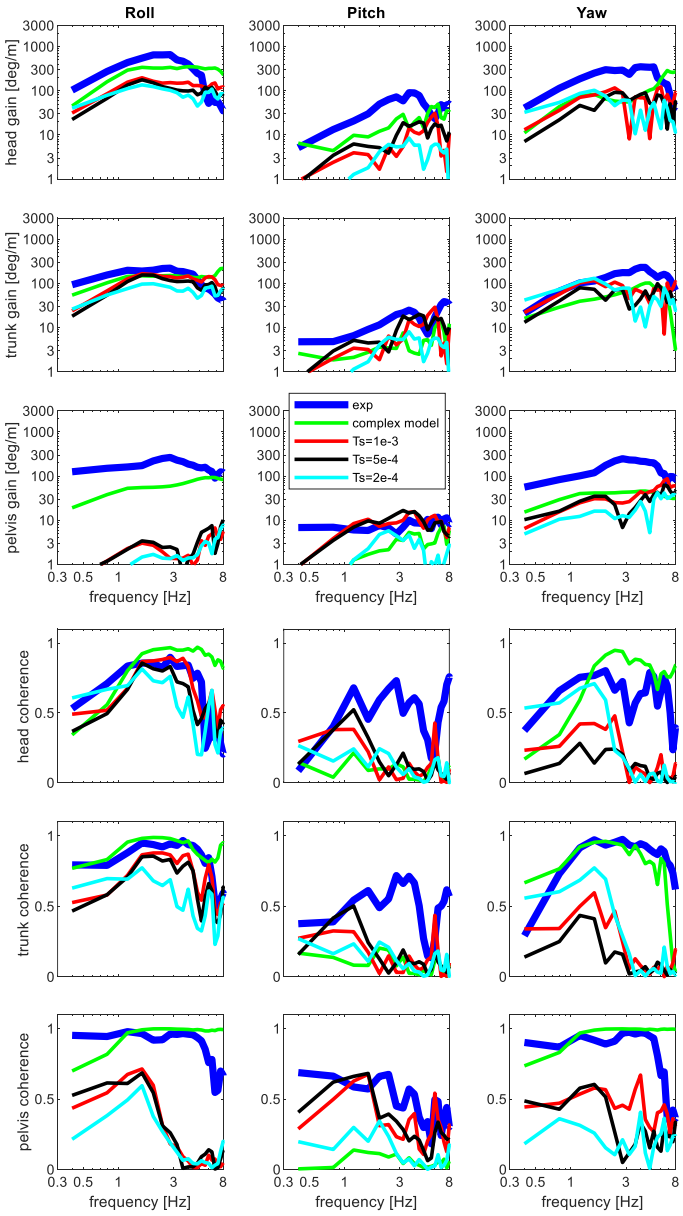

Figure 5.4 Plots of lateral seat motion validation with different time steps. Gains (upper 3 rows) and coherence (lower 3 rows) for head, trunk and pelvis in roll motion (left column), pitch motion (middle column) and yaw motion (right column)

Fig 5.3 and Fig 5.4 shows resultant plot of lateral seat motion. New models of all time steps do not have perfect match similar to x gain of trunk in fore-aft seat motion. The relative better fit takes place at y gains of head and pelvis and roll gain of trunk. Other roll gains and yaw gains of SHM have similar shape with experimental data but they are much lower. None of models fit well to y gain of trunk. In low frequency domain, all SHM of different time steps have high y coherence, but they drop after 3Hz. This law is also applied to roll coherence of pelvis, yaw coherence of head and trunk. Similar to pitch coherence in fore-aft seat motion, model of 1e-3, as longest time step, has highest roll coherence of all bodies.

As to non-required gains, it is outstanding that models of 1e-3 and 5e-4 have good fit

to z gain of trunk and capture the peak response of experimental data while model of 2e-4 is much worse. These two models also fit better than AHM in z gains. In pitch gains, these two models can partly capture experimental response in trunk and pelvis. In z displacement and pitch motion, 2e-4 is the worst model because it has worst fit in gains and lowest coherence.

5.3 Final result of vertical seat motion

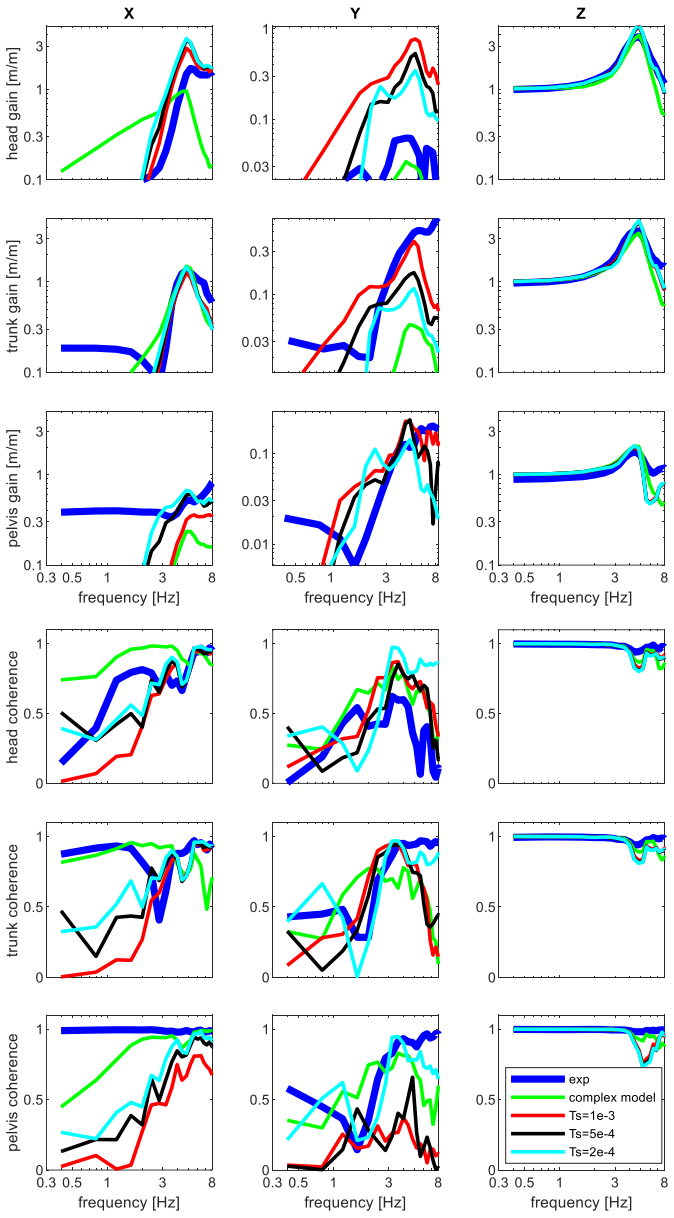

Figure 5.5 Plots of vertical seat motion validation with different time steps. Gains (upper 3 rows) and coherence (lower 3 rows) for head, trunk and pelvis in x displacement (left column), y displacement (middle column) and z displacement (right column).

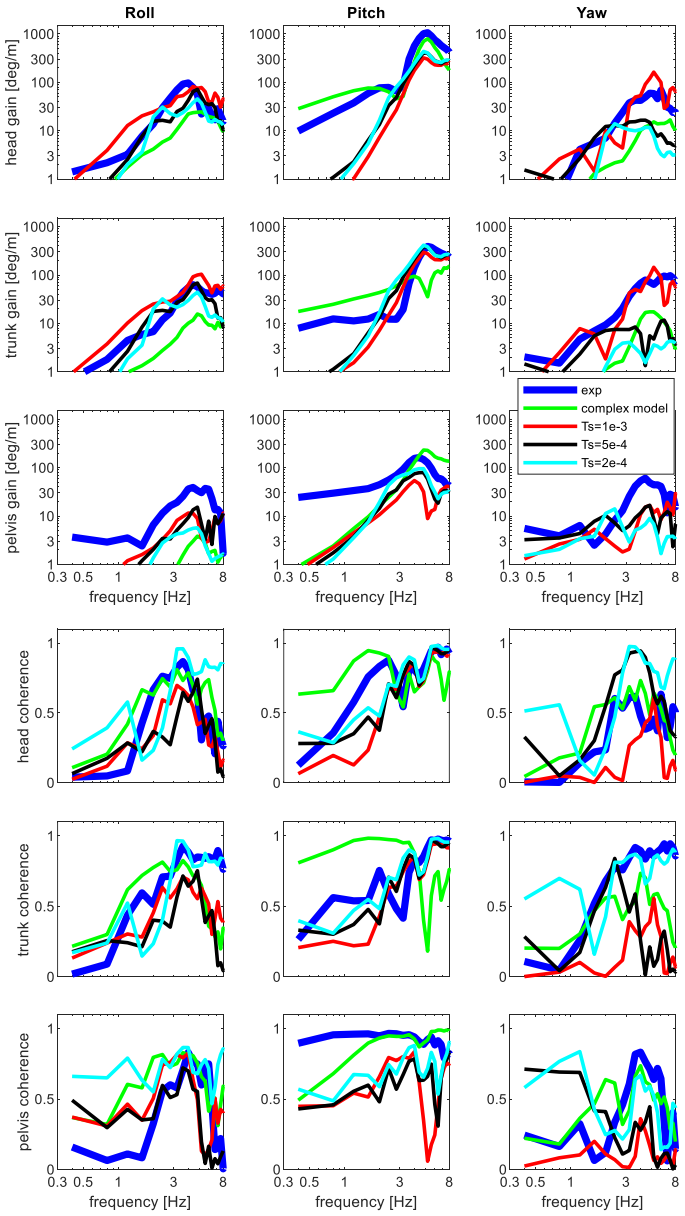

Figure 5.6 Plots of vertical seat motion validation with different time steps. Gains (upper 3 rows) and coherence (lower 3 rows) for head, trunk and pelvis in roll motion (left column), pitch motion (middle column) and yaw motion (right column)

Fig 5.6 and Fig 5.7 shows resultant plot of vertical seat motion. Same as old models, models of all time steps fit well with experimental data in z gains. Z coherences are also high as experimental data.

As to non-require gains, all models fit well with experimental data in x gains and x coherence of head and trunk in the interval [3 8]Hz. In this interval, models of 2e-4 also fit well in x gains of pelvis. In roll gains, three SHM are also able to capture the experimental responses in head and trunk, but a bit lower in pelvis. In pitch gains, three SHM can capture the peek response in trunk and pelvis. The good fit in pitch gains only applies to the interval [3 8]Hz. Model of 1e-3 have best fit among SHM in yaw gains of head and pelvis. However, it has lowest coherences.

5.4 CPU of different time step

Models of different time steps cost different total time to run the simulation. Shorter time step leads to longer total time. Details of CPU time of models in fore-aft seat motion are shown in Table 5-1 (See Appendix C for lateral and vertical seat motion). All simulations are finished under the same computer configuration. These tables are samples of single simulation running. The running times are not necessarily maintained unchanged.

According to Table 5-1, the SHM does not spend any CPU on FE-relative subjects. The main subject spending CPU is total multibody because the SHM is a multibody model. Table 5-1 illustrates that the AHM spends more CPU time on multibody than SHM. Moreover, the AHM spends more than half total CPU time on FE subjects. The factors that SHM are faster than AHM depends on the time step. Models of 1e-3s, 5e-4 and 2e-3 are about factors 116, 88 and 47 faster than AHM, respectively.

Table 5-1 CPU time of models in fore-aft seat motion

Subject	CPU time (s)			
	SHM of time step = 1e-3s	SHM of time step = 5e-4s	SHM of time step = 2e-3s	AHM of time step = 5e-5s
Initialisation	0 (0%)	0.1 (0%)	0.1 (0%)	4.3(0%)
Element processing	0 (0%)	0 (0%)	0 (0%)	1866.0 (11%)
Element/Facet-Node/Vertex contact	0 (0%)	0 (0%)	0 (0%)	3639.7 (21%)
Multibody-Node/Vertex contact	0 (0%)	0 (0%)	0 (0%)	1184.2 (7%)
Supports	0 (0%)	0 (0%)	0 (0%)	1509.2 (9%)
External loads	0 (0%)	0 (0%)	0 (0%)	6.6 (0%)
Spowelds/FE rigid bodies/constraints	0 (0%)	0 (0%)	0 (0%)	2.4 (0%)
FE time integration	0 (0%)	0 (0%)	0 (0%)	44.9 (0%)
Total Finite Element	0 (0%)	0 (0%)	0 (0%)	9999.9 (58%)
Total Multi Body	138.0 (93%)	179.1 (91%)	323.7 (91%)	6140.2 (36%)
External program in coupling	5.5 (4%)	10.2 (5%)	26.5 (5%)	1107.9 (6%)
Output	4.2 (3%)	5.3 (3%)	10.6 (3%)	14.6 (0%)
Filtering and injury	1.1 (1%)	1.6 (1%)	2.7 (1%)	0 (0%)
Total	148.8 (100%)	196.3 (100%)	363.6 (100%)	17266.9 (100%)

5.5 New criterion formulas for cost function of identification

In this thesis, three steps of optimization are used to find the optimum. As the first step, the manual tuning is conducted to get a good initialization for the optimization. However, due to the complexity of the optimization problem, gradient search fails to find the optimum values, not able to modify the initial parameters. The complexity is caused by the cost function, which is the criterion to determine how the model is close to experimental data. What's more, the formulas of current criterion do not show better fit for lower value. During grid search, sometimes it happens that the lowest

evaluation gives a bad evaluation. This leads to the selection of grid node of second or even third lowest values. Therefore, a new criterion needs to be conduct.

The current criterion is influenced by the response out of interesting interval. In order to solve this, a potential improvement is to simplify this cost function. The new formulas to calculate criterion is interpreted below.

Same as original ones, in each seat motion, the gain of experiment as function of frequency is denoted as $G_{ex}(f)$ and the gain of model as function of frequency is denoted as $G_{md}(f)$. However, the domain of these response functions are now restricted in interesting interval. The interested interval from now on is restricted in (0,8]Hz. A relative error of gains is as expression:

$$e_n(f) = (G_{ex}(f) - G_{md}(f))^2 / G_{ex}(f) \tag{6.1}$$

where n represents different gains, same as initial criterion. The criterion of each seat motion is expressed as:

$$e_x = \sqrt{\frac{\sum_{n=1,5} \sum_{f=0.3}^{N} e_n(f)}{N}} \tag{6.2}$$

$$e_y = \sqrt{\frac{\sum_{n=2,4,6} \sum_{f=0.3}^{N} e_n(f)}{N}} \tag{6.3}$$

$$e_z = \sqrt{\frac{\sum_{n=3} \sum_{f=0.3}^{N} e_n(f)}{N}} \tag{6.4}$$

where N is number of data points. These criterions are the cost function of each seat motion for optimization. They are some kinds of root-mean-square of relative errors. By using such definition of criterion, relative errors in interesting frequency interval could be directly utilized for optimization without influence from other frequencies. An example illustrates this new criterion is more suitable for this parameter identification. During the grid search of parameters of Shy and Dhy in fore-aft seat motion, the prediction plots of lowest criterion apparently indicate an infeasible fit, thus another pair of Shy and Dhy is selected. Fig. 5.7 shows the prediction plots of parameter pairs of infeasible lowest initial criterion, the selection based on initial criterion and lowest criterion based on new formula.

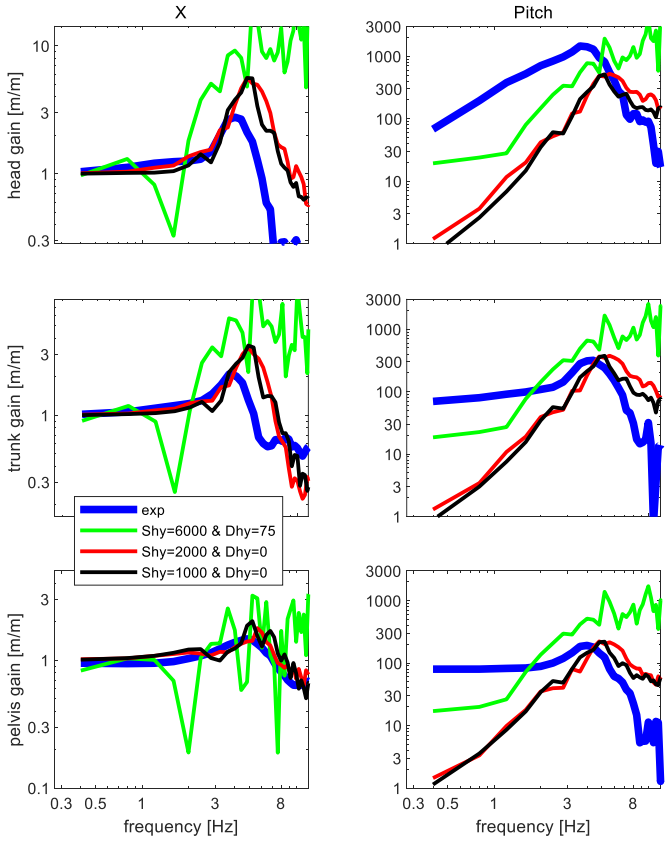

Figure 5.7 Prediction plots of fore-aft seat motion validation during grid search. Gains for head, trunk and pelvis in roll motion (left column) and pitch motion (right column). Green lines stand for the parameter pairs of lowest initial criterion, red lines stands for the parameter pairs of selected one based on initial criterion and black lines stand for the parameter pairs of lowest criterion based on new formula.

6. Discussion

6.1 Discussion on grid search and new criterion formulas

Compared with result of gradient search, the done grid search is better but not perfect, either. It is time-consuming to do one grid evaluation. That is the reason why the current resolution is set large. Smaller resolution leads to higher probability to find global optimum, but times of evaluation also increase. Therefore, due to the current large resolution, the output parameter values actually are relatively better values but not best values. If condition allows, smaller resolution could be done to find better optimum.

The boundaries of grids are also able to be redefined. The boundaries of each parameter are approximated by initial values of corresponding parameter. A different range of grid is valid as long as it covers the initial parameter values. Moreover, according to Fig. 4.2, the minimum of parameter pair (Swt and Dwt) trends to take place at outside the current grid. Therefore, grid Swt and Dwt should be extended.

Every grid evaluation only applies to two parameters. It could lead to a consequence that the outcome values of after parameter tuning may affect the result of previous tuning. Outcome values of previous parameters are probably not the optimum any more. Therefore, doing a grid search loop may help solve this. After all grids are evaluated once, repeating the grid search again and obtain smaller values of new criterions. When the difference of criterions is smaller than a specific threshold, stop the loop and current parameter values are regarded the best ones. Such algorithm may improve the parameter identification.

Parameters pair with lowest initial criterion (the one represented by green lines in Fig. 5.7) produces higher criterion based on the new formulas. The minimum of new criterion also indicates a pair of parameters of better fit (the one represented by black lines in Fig. 5.7). According to Fig. 6.1, the new formulas make surface plot of new criterion smoother than the old one, though it is not perfectly smooth. Another improvement is it can indicate all infeasible fit by giving high values of criterion.

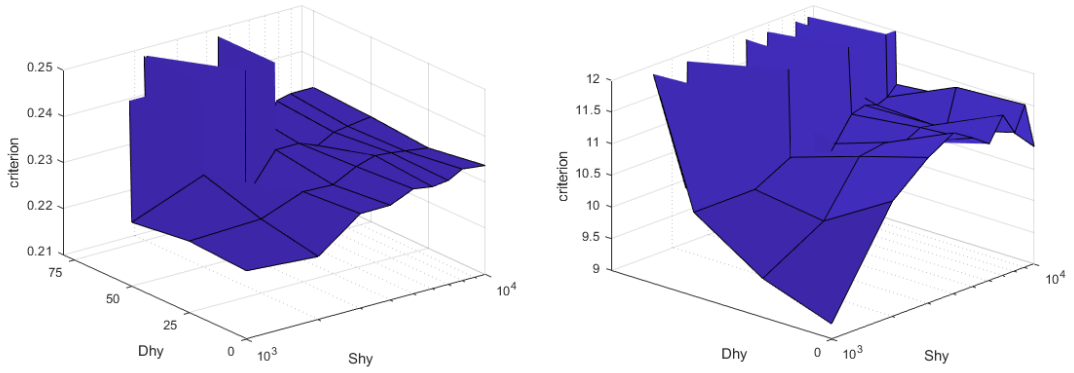

Figure 6.1 Nodes of grid search and result surface plots of criterions for parameters Shy and Dhy in fore-aft seat motion by initial formulas (left) and new formulas (right)

6.2 Comparison between outcome values of parameters and values in literature

A comparison table of best parameters from grid search and parameters from literature is listed below (Table 6-1):

Table 6-1 Comparison between outcome of grid search and Wu's proposal mode

Parameters	Values outcome from grid search	Values from Wu [24]	
Swx	500	956.7	
Dwx	0	0.0019	
Swy	80000	Na	
Dwy	0	Na	
Swz	50	Na	
Dwz	10	Na	
Strx	40000	80.6	
Dtrx	0	0	
Stry	3000	Na	
Dtry	0	Na	
Strz	60	Na	
Dtrz	300	Na	
Shx	60000	14400	
Dhx	50	92800	
Shy	2000	Na	
Dhy	0	Na	
Shz	2000	Na	
Dhz	20	Na	
Snx	8000	144	
Dnx	20	0.5734	
Sny	9000	Na	
Dny	50	Na	
Snz	1000	Na	
Dnz	40	Na	
Swt	50000	81100	
Dwt	0	1100	
Sp	95000	lateral	2860
		vertical	48970
Ds	750	lateral	399.3
		vertical	0.17
Sto	40000	lower lateral	1000
		lower vertical	1000
		upper lateral	1280
		upper vertical	1000

Table 6-1 (continued)

Parameters	Values outcome from grid search	Values from Wu [24]	
Dsb	1600	lower lateral	7.1
		lower vertical	0
		upper lateral	60.8
		upper vertical	51.2
Sth	10000	lateral	4800
		vertical	153900
Dss	1000	lateral	0
		vertical	0.0018

In Wu's model [24], body segments are connected by translational joints in lateral and vertical directions and revolute joints around fore-aft direction. His human model is excited by a vibration combined by lateral, vertical and roll direction. In SHM, body segments are connected by revolute and spherical joints. Translational joint is only used in waist along vertical direction. This SHM is separately excited by fore-aft, lateral and vertical vibrations. All joints in these two models are linear. Even they have similar components, same parameters are assigned values of considerable difference. The reason of such phenomenon is that human body is a complex system. Human joints are unable to generally be modeled by one single or combined linear set of spring and dampers. The vehicle vibration, posture of human body and even what the human see are factors decide the nonlinearity of joints. Therefore, a comprehensive human model with adaptive parameters still needs to be developed.

6.3 Effects of time steps

Normally shorter time steps lead to better result of a model. However, it is not applied to this SHM. In the gain fitting, model of 2e-4 fits best in head's yaw gain in fore-aft seat motion (Fig. 5.2) while models of longer time steps (1e-3s and 5e-4s) fit best in trunk's z gain in lateral seat motion (Fig. 5.3). Due to the big difference between models of two longest time steps and model of shortest time step in lateral seat motion, two models of shorter time steps (1e-4s and 5e-5s) are added into comparison. According to Fig. 6.2 and Fig. 6.3, models of 2e-4s, 1e-4s and 5e-5s are converged to almost the same result. It could be concluded that time steps basically do not affect the prediction when it is smaller than 2e-4s.

Overall, model of 2e-4 works better in fore-aft seat motion and model of time steps 1e-3 works better in lateral seat motion. Models of these two shortest time steps fit better in vertical seat motion. One possible reason of such result is that the parameter tuning of this model is based on time step equal to 1e-3s. Models of other time steps do not provide better overall prediction even though the shorter time step theoretically leads to more realistic result. Therefore, in order to get better model, shorter time steps should be also applied to the parameter identification even it cost more time.

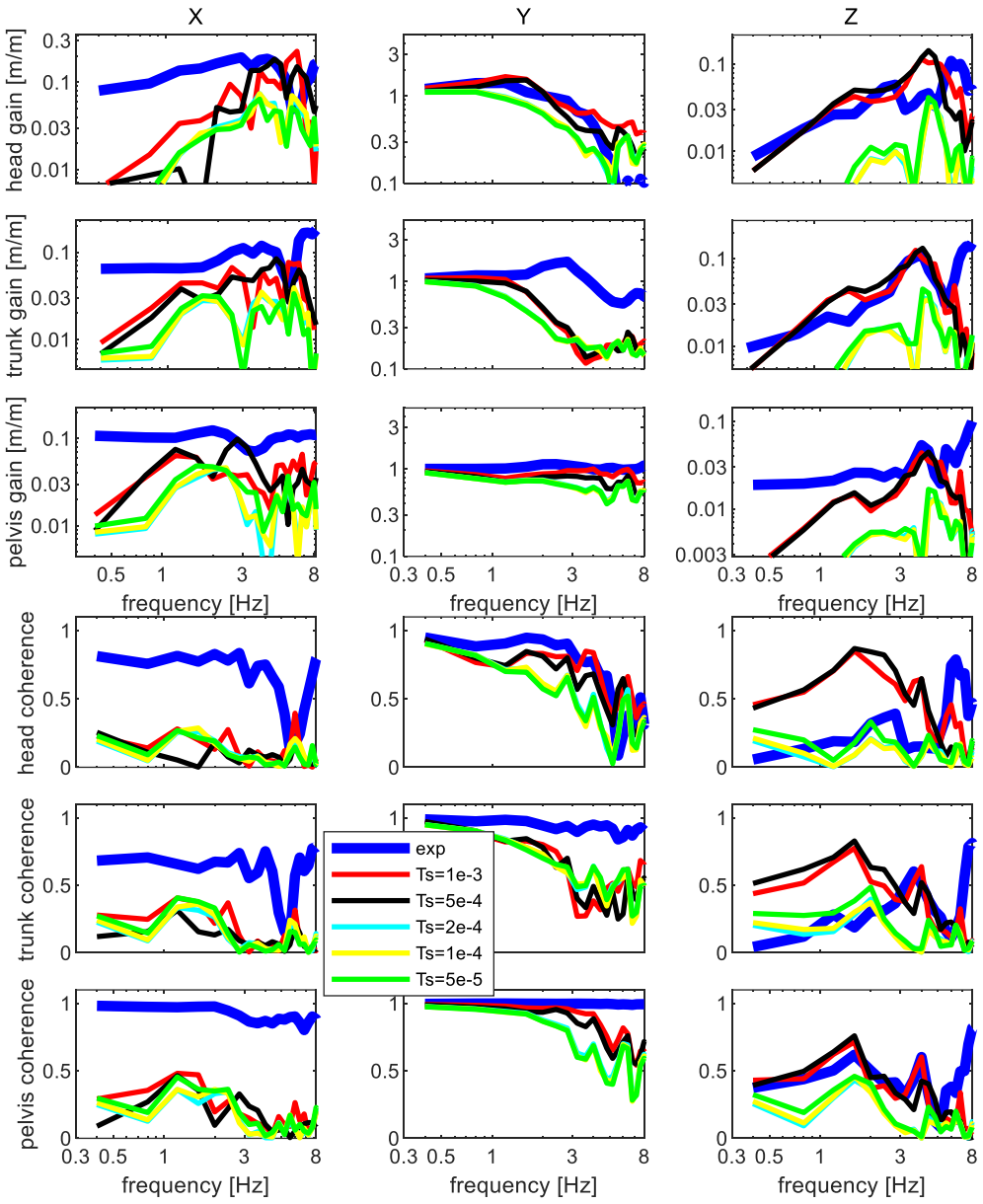

Figure 6.2 Plots of lateral seat motion validation with more different time steps. Gains (upper 3 rows) and coherence (lower 3 rows) for head, trunk and pelvis in x displacement (left column), y displacement (middle column) and z displacement (right column).

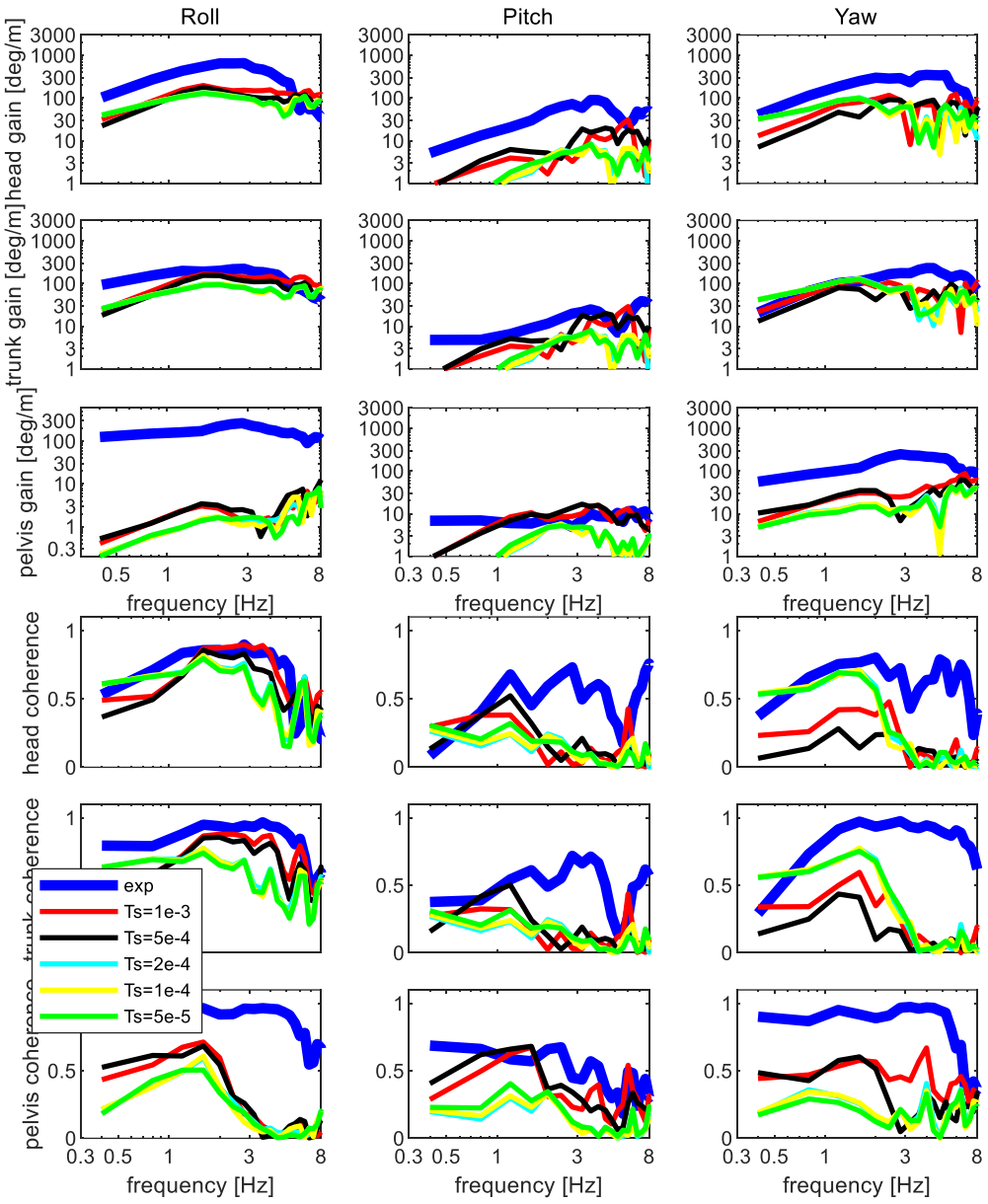

Figure 6.3 Plots of lateral seat motion validation with more different time steps. Gains (upper 3 rows) and coherence (lower 3 rows) for head, trunk and pelvis in roll motion (left column), pitch motion (middle column) and yaw motion (right column)

6.4 Effects of model geometry and lack of translational waist

In order to find out if making the torso segments rounder and changing back rest improve the prediction, models of new and old geometries are compared. Replacing the translation of waist by rigid (in vertical direction) waist is assumed to be more realistic. Therefore, normal models of new and old geometries, and the model of new geometry without translational joint (no-waist model below) in waist are put together to compare (Fig. 6.4, 6.5 and 6.6).

Overall, three models do not have large difference in gain fitting. However, no-waist

model has bad fit in z gains in vertical seat motion. The reason is that the parameter values are identified based on initial model structure. Moreover, z displacement is sensitive to vertical translational stiffness and damping. Therefore, bias exclusively takes place at z displacement.

According to Fig. 6.4, 6.5 and 6.6, old model has lowest coherence, whose reason is interpreted in chapter 4.4. No-waist model has highest coherences of all body segments in vertical seat motion. That is because this model is more rigid on vertical direction than normal SHM. The body system is more linear and seat vibration is better transmitted to body segments. Overall, normal SHM of new geometry is best of these three models.

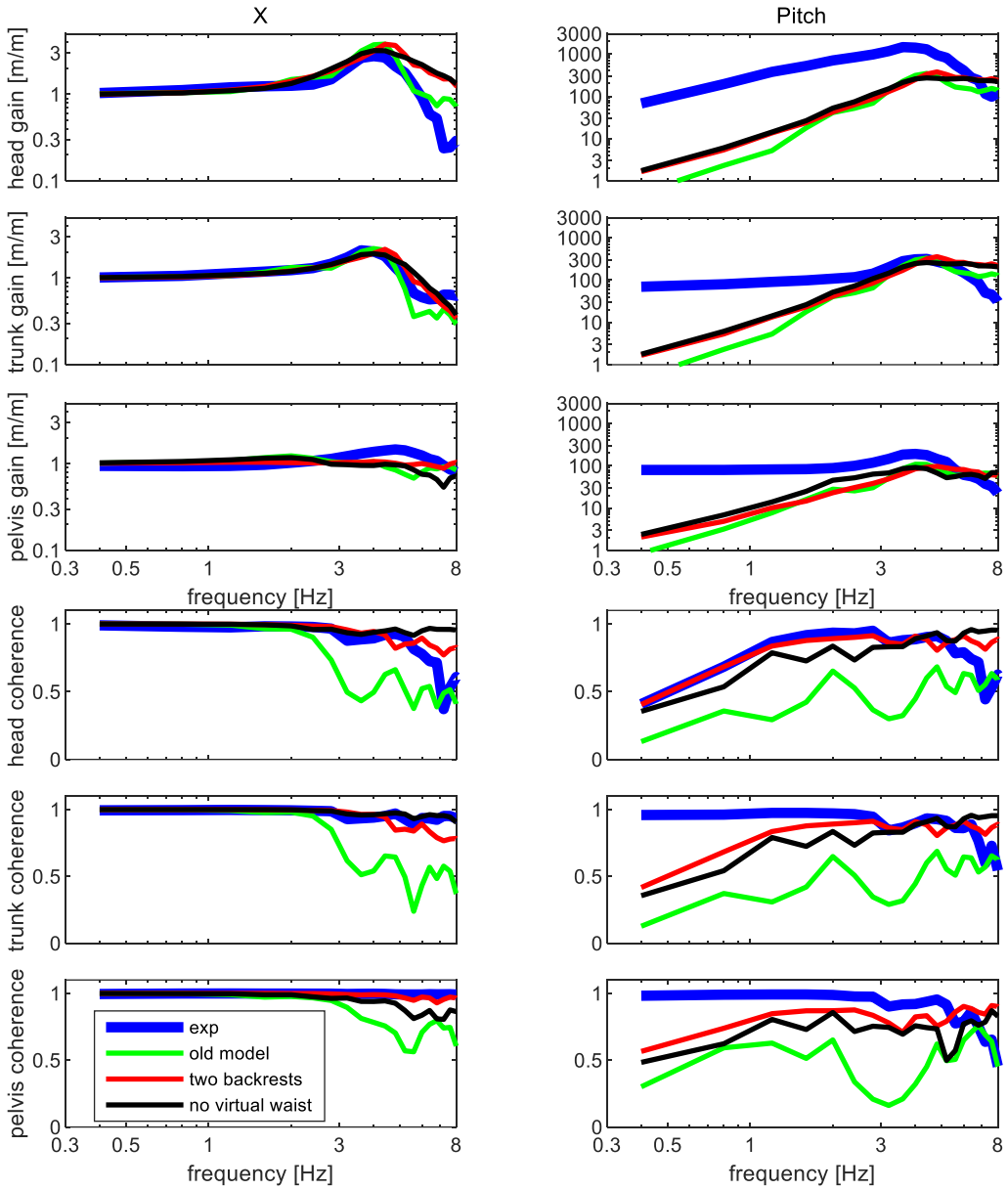

Figure 6.4 Plots of fore-aft seat motion validation with different geometry. Gains (upper 3 rows) and coherence (lower 3 rows) for head, trunk and pelvis in x displacement (left column) and pitch motion (right column). Time step = 1e-3s.

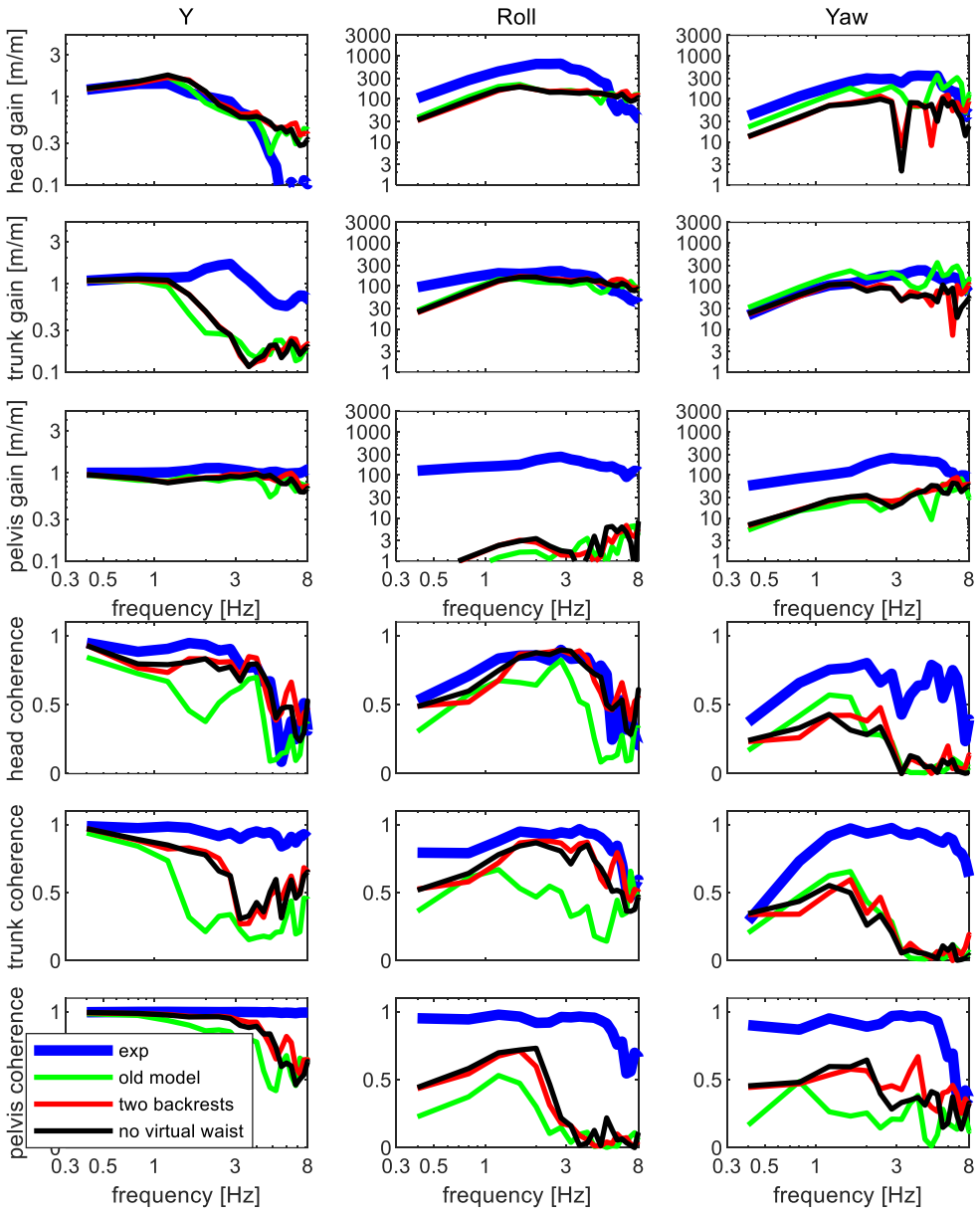

Figure 6.5 Plots of lateral seat motion validation with more different time steps. Gains (upper 3 rows) and coherence (lower 3 rows) for head, trunk and pelvis in y displacement (left column), roll motion (middle column) and pitch motion (right column). Time step = 1e-3s.

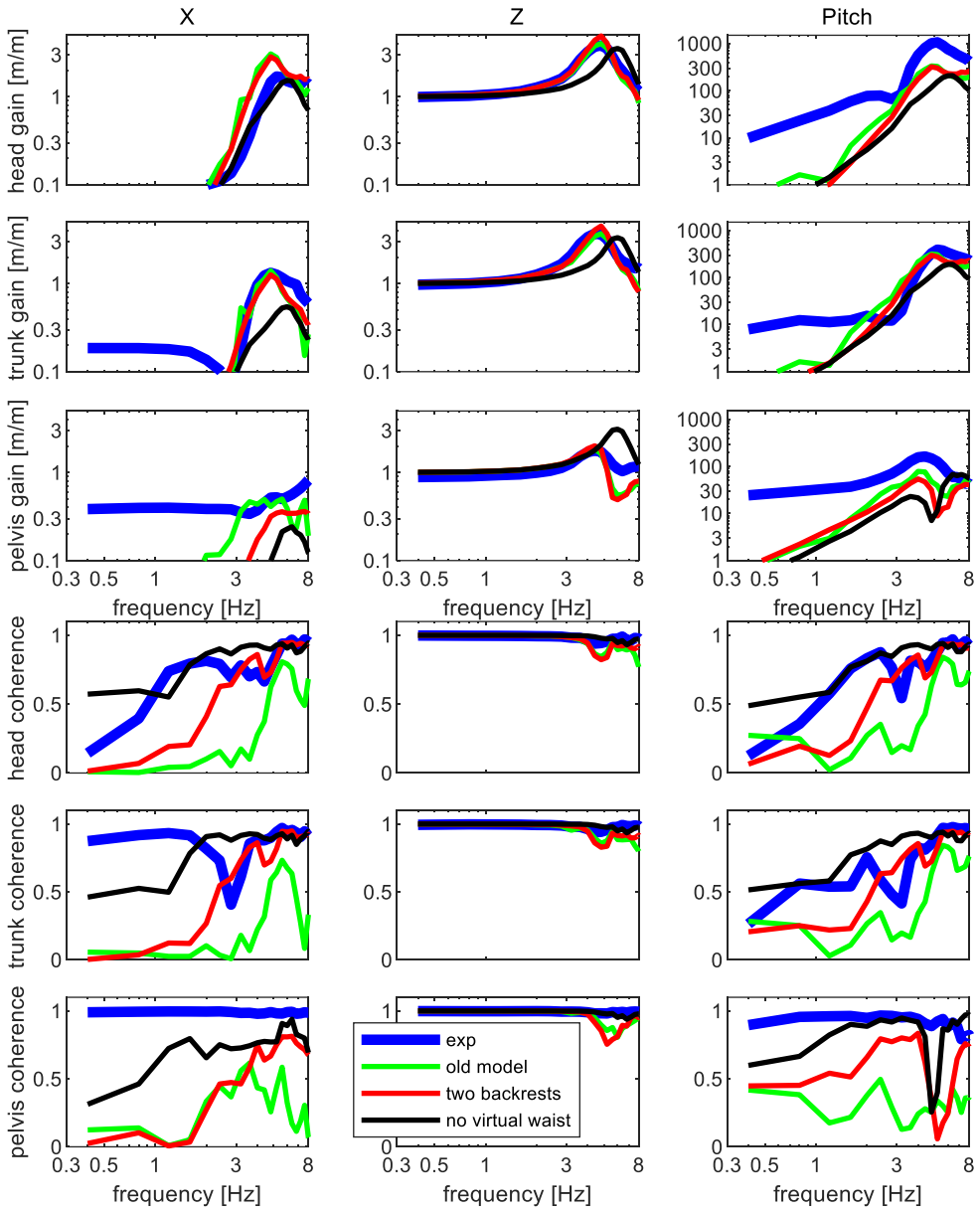

Figure 6.6 Plots of vertical seat motion validation with more different time steps. Gains (upper 3 rows) and coherence (lower 3 rows) for head, trunk and pelvis in x displacement (left column), z displacement (middle column) and yaw motion (right column). Time step = 1e-3s.

6.5 Asymmetry of the SHM

The model and environment shall have no noise ideally. However, lateral, roll and yaw movements occur in fore-aft seat motion (fore-aft vibration). These movements are supposed to not happen due to the ideal conditions. The possible reason is that the human model is not located at the center of seat. The seat pan and backrest are modeled as ellipsoid, which means their surfaces are not ideally flat. Due to the penetration mechanism of force calculation, the force of seat applied on human model is not in mid-sagittal plane as long as mid-sagittal planes of seat and human model are

not absolute consistent. Such deflected force will cause the human model to do lateral, roll and yaw movement.

6.6 Discussion on required gains that could be improved

Most required gains have good fit with experimental data while some other obviously do not. Pitch motion of head, trunk and pelvis have lower gains in low frequency domain in fore-aft seat motion. In lateral seat motion, gain of y displacement of model's trunk starts to drop at 1.5Hz while experimental data starts to increases. Also in lateral seat motion, gains of roll and yaw motion of model's pelvis are both apparently lower than experimental data.

For pitch motions in fore-aft seat motion, nonlinearity of stiffness and damping coefficient could be the reason of bad fit. In reality, participants of experiments were actively leaning on the backrest. The rotational stiffness of human joints around y axis is always changing to keep the human leaning on backrest. However, the SHM is a passive dummy. The current model lumps muscular stabilization using linear springs, which means its stiffness is maintained unchanged. In low frequency domain, the stiffness is too small to give body segments high gains because it does not actively lean on backrest. This could also explain bad fit of y gain of model's trunk. The active human trends to actively keep neutral position. However, without support on lateral direction and inertia, the human always over-acting, which cause high gains on lateral direction. Modeling actual muscles can enhance realism by including reflexive delays and non-linear muscle dynamics. Joint stiffening could be achieved by using muscle feedback. For space stabilization of head, more advanced control scheme are needed to capture vestibular and visual feedback. Therefore, adding line muscle elements in SHM is a solution.

For roll of pelvis in lateral seat motion, the shape could be a reason for lower gain. Buttock is the contact point between pelvis and seat pan. Pelvis is modeled as an ellipsoid with high degrees. Its surface is too flat to roll. However, real buttock is rounder. Therefore, making degrees of pelvis ellipsoid lower or shaping the pelvis more realistic could be a solution.

For yaw motion of pelvis in lateral seat motion, a possible solution is to adjust torso's center of mass. In current SHM model, the projections of torso's center of mass and pelvis on x-y plane are close. Thus forces produced by torso's inertia cannot provide large torque. Therefore, making torso's center of mass close to the back or placing pelvis's center of mass forward probably improve yaw gain's fit.

7. Conclusion and recommendations

7.1 Conclusion

Referring to the human body in literature, a simplified multibody human body model is constructed and developed. This model is made up with multiple rigid bodies and joints connect them together. Vibrations from fore-aft, lateral and vertical could be applied on this model. Gradient search is not suitable since the optimization problem is not smooth. The model is validated by experiment data and optimized by grid search. The grid search also shows that the current cost function is not perfectly suitable. Compared to AHM, the SHM gets similar or even better human responses. This SHM takes no more than 10 minutes to simulate 30 seconds, which could be most 116 faster than AHM who takes about 1 hours. The result plots shows that the SHM could replace AHM at required gains except pitch gains in fore-aft seat motion, roll gain of pelvis in lateral seat motion. Different lengths of time steps of SHM are compared. It shows that shorter time steps do not necessarily give more accurate result for this SHM which is tuned based one time step equal to 1e-3.

7.2 Future improvement

Because lower value of criterion does not necessarily indicate better fit, new formulas of criterion as cost function of optimization should be conducted. Suggestion in chapter 6.1 is worth being tried. Since this SHM is only applicable to the vibrations from different single directions, it is not realistic enough to simulate a human body suffering combined vibration of vehicle. An experiment about human subject responding to combined vibration could be done to collect data for Madymo multibody human body models optimization. Such human body model would be more comprehensively validated.

The current SHM is made up with rigid bodies. However, the human body is not rigid because skin and issue is soft. Although skin element in Madymo, as a finite element, is so complex that takes longer time to simulate, deformable elements could be used to build up the human bodies.

The current SHM only have linear spring and dampers in joints, thus it is a dummy but not an active model. Some magnificent muscle elements could be added to connect body segments. Due to the restriction of human body, stiffness of body joints varies from the position of body segments, which means the stiffness is nonlinear. Adding muscles and nonlinear stiffness could help model more realistic, which potentially helps improve the model.

Another way to make the model close to real human is to shape the SHM more human-like. This could be achieved by defining a large amount of rigid bodies and ellipsoid surfaces.

References

[1] Desai, R., Guha, A. and Seshu, P., 2021. A comparison of different models of passive seat suspensions. *Proceedings of the Institution of Mechanical Engineers, Part D: Journal of Automobile Engineering*, p.095440702199092.

[2] Rupp, T., Ehlers, W., Karajan, N., Günther, M., & Schmitt, S. (2015). A forward dynamics simulation of human lumbar spine flexion predicting the load sharing of intervertebral discs, ligaments, and muscles. *Biomechanics And Modeling In Mechanobiology*, *14*(5), 1081-1105. doi: 10.1007/s10237-015-0656-2

[3] Himmetoglu, S., Acar, M., Bouazza-Marouf, K. and Taylor, A., 2009. A multibody human model for rear-impact simulation. *Proceedings of the Institution of Mechanical Engineers, Part D: Journal of Automobile Engineering*, 223(5), pp.623-638.

[4] Bova, M., Massaro, M. and Petrone, N., 2020. A Three-Dimensional Parametric Biomechanical Rider Model for Multibody Applications. *Applied Sciences*, 10(13), p.4509.

[5] Zheng, G., Qiu, Y. and Griffin, M., 2011. An analytic model of the in-line and cross-axis apparent mass of the seated human body exposed to vertical vibration with and without a backrest. *Journal of Sound and Vibration*, 330(26), pp.6509-6525.

[6] Desai, R., Guha, A. and Seshu, P., 2021. An appropriate biomechanical model of seated human subjects exposed to whole-body vibration. *Proceedings of the Institution of Mechanical Engineers, Part K: Journal of Multi-body Dynamics*, 235(4), pp.586-601.

[7] Sharma, R., Sharma, S., Sharma, S., Sharma, N. and Singh, G., 2021. Analysis of bio-dynamic model of seated human subject and optimisation of the passenger ride comfort for three-wheel vehicle using random search technique. *Proceedings of the Institution of Mechanical Engineers, Part K: Journal of Multi-body Dynamics*, 235(1), pp.106-121.

[8] Teng, T., Chang, F., Liu, Y. and Peng, C., 2008. Analysis of dynamic response of vehicle occupant in frontal crash using multibody dynamics method. *Mathematical and Computer Modelling*, 48(11-12), pp.1724-1736.

[9] Teng, T., Chang, F. and Peng, C., 2006. Analysis of human body response to vibration using multibody dynamics method. *Proceedings of the Institution of Mechanical Engineers, Part K: Journal of Multi-body Dynamics*, 220(3), pp.191-202.

[10] Rodrigo, S., Ambrósio, J., Tavares da Silva, M. and Penisi, O., 2008. Analysis of Human Gait Based on Multibody Formulations and Optimization Tools#. *Mechanics Based Design of Structures and Machines*, 36(4), pp.446-477.

[11] Barbeau, R., Weisser, T., Dupuis, R., Aubry, É. and Baudu, S., 2019. Assessment of the impact of sub-components on the dynamic response of a coupled human body/automotive seat system. *Journal of Sound and Vibration*, 459, p.114846.

[12] Govindan, R., Saran, V. and Harsha, S., 2021. Biodynamic response analysis of semi-supine human under varying vertical excitations. *International Journal of Industrial Ergonomics*, 85, p.103195.

[13] Cho, Y. and Yoon, Y., 2001. Biomechanical model of human on seat with backrest for evaluating ride quality. *International Journal of Industrial Ergonomics*, 27(5), pp.331-345.

[14] Azizi, Y., Puri, T., Bajaj, A. and Davies, P., 2015. Development of a Multibody Model to Predict the Settling Point and Interfacial Pressure Distribution in a Seat–Occupant

System. *Journal of Computational and Nonlinear Dynamics*, 10(3).
[15] Mohajer, N., Abdi, H., Nahavandi, S. and Nelson, K., 2017. Directional and sectional ride comfort estimation using an integrated human biomechanical-seat foam model. *Journal of Sound and Vibration*, 403, pp.38-58.
[16] Kumbhar, Prasad & Xu, Peijun& Yang, Jingzhou. (2013). Evaluation of Human Body Response for Different Vehicle Seats Using a Multibody Biodynamic Model. SAE Technical Papers. 2. 10.4271/2013-01-0994.
[17] Vadiraj, B., Omkar, S., Kandagal, S. and Kiran, M., 2012. Human Response Characteristics to Impact Conditions During Spacecraft Takeoff and Impact Landing. *International Journal of Aerospace Innovations*, 4(3-4), pp.95-102.
[18] Teng, T., Liang, C., Huang, H. and Peng, C., 2012. Kane's method applied to the simulation of a vehicle occupant in side impact. *Proceedings of the Institution of Mechanical Engineers, Part K: Journal of Multi-body Dynamics*, 226(3), pp.183-196.
[19] Liu, C. and Qiu, Y., 2020. Localised apparent masses over the interface between a seated human body and a soft seat during vertical whole-body vibration. *Journal of Biomechanics*, 109, p.109887.
[20] Govindan, R., Saran, V. and Harsha, S., 2020. Low-frequency vibration analysis of human body in semi-supine posture exposed to vertical excitation. *European Journal of Mechanics - A/Solids*, 80, p.103906.
[21] LIANG, C. and CHIANG, C., 2008. Modeling of a Seated Human Body Exposed to Vertical Vibrations in Various Automotive Postures. *Industrial Health*, 46(2), pp.125-137.
[22] Desai, R., Guha, A. and Seshu, P., 2021. Modelling and simulation of active and passive seat suspensions for vibration attenuation of vehicle occupants. *International Journal of Dynamics and Control*, 9(4), pp.1423-1443.
[23] Desai, R., Guha, A. and Seshu, P., 2021. Modelling and simulation of an integrated human-vehicle system with nonlinear cushion contact force. *Simulation Modelling Practice and Theory*, 106, p.102206.
[24] Wu, J. and Qiu, Y., 2020. Modelling of seated human body exposed to combined vertical, lateral and roll vibrations. *Journal of Sound and Vibration*, 485, p.115509.
[25] Qiu, Y. and Griffin, M., 2010. Modelling the fore-and-aft apparent mass of the human body and the transmissibility of seat backrests. *Vehicle System Dynamics*, 49(5), pp.703-722.
[26] Desai, R., Guha, A. and Seshu, P., 2020. Multibody modelling of the human body for vibration induced direct and cross-axis seat to head transmissibility. *Proceedings of the Institution of Mechanical Engineers, Part C: Journal of Mechanical Engineering Science*, 235(17), pp.3146-3161.
[27] Liu, C. and Qiu, Y., 2020. Nonlinearity in the localised apparent masses of the seated human body exposed to vertical vibration. *Mechanical Systems and Signal Processing*, 135, p.106394.
[28] Amirouche, F. and Ider, S., 1988. Simulation and analysis of a biodynamic human model subjected to low accelerations—A correlation study. *Journal of Sound and Vibration*, 123(2), pp.281-292.
[29] Yu, Z., Zhao, Q., Yang, J., Xia, Y. and Ma, Y., 2021. Uncoupled spatial biodynamic model for seated humans exposed to vibration-development and validation. *International Journal of Industrial Ergonomics*, 85, p.103171.

[30] Winter, D., 2009. *Biomechanics and motor control of human movement*. Hoboken, NJ: Wiley.
[31] Siemens Digital Industries Software., 2020. *Siemens Madymo Reference Manual.* Version 2020.2.
[32] Siemens Digital Industries Software., 2020. *Siemens MadymoHuman Body Model Manual.*Release 2020.2.
[33] Mirakhorlo, M., Kluft, N., Desai, R., Cvetković, M., Irmak, T., Shyrokau, B. and Happee, R., 2022. Simulating 3D Human Postural Stabilization in Vibration and Dynamic Driving. *Applied Sciences*, 12(13), p.6657.

Appendix A. Result plots of manual tuning

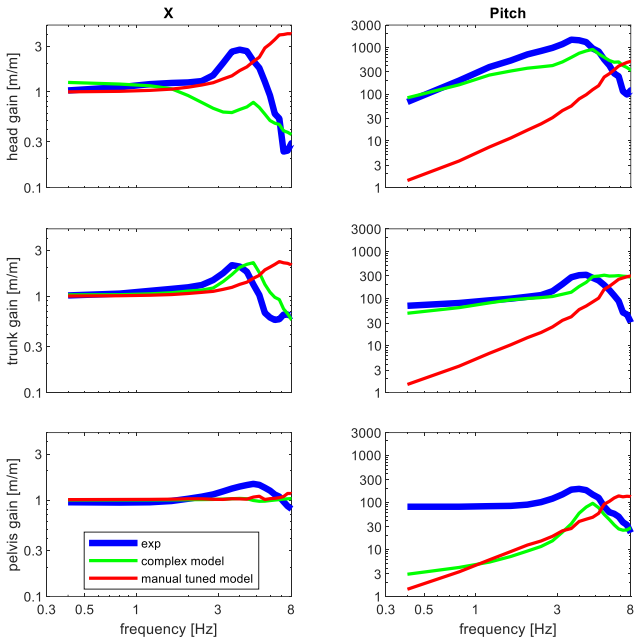

Figure A.1 Plots of fore-aft seat motion validation by manual tuning. Gains (upper 3 rows) and coherence (lower 3 rows) for head, trunk and pelvis in x displacement (left column) and pitch motion (right column).

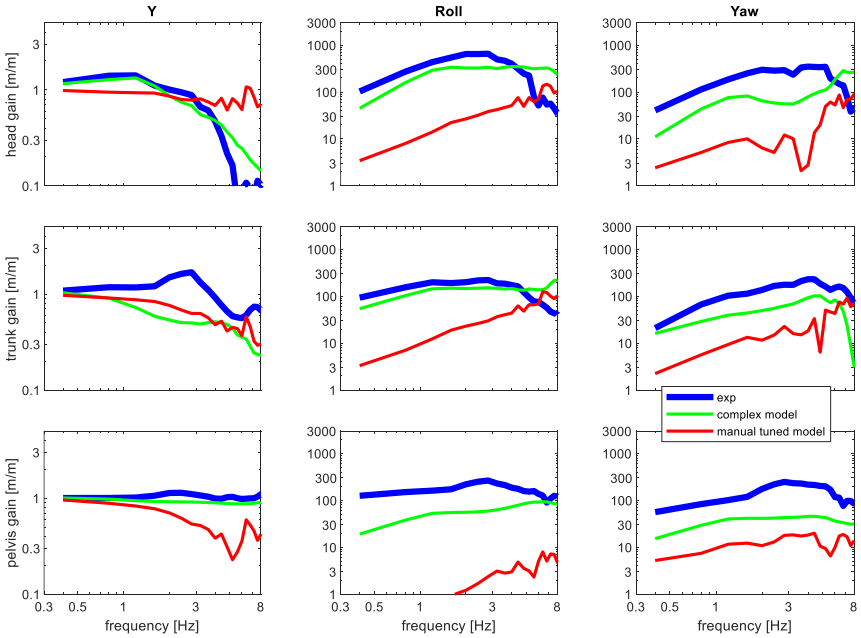

Figure A.2 Plots of lateral seat motion validation by manual tuning. Gains (upper 3 rows) and coherence (lower 3 rows) for head, trunk and pelvis in y displacement (left column), roll motion and yaw motion (right column).

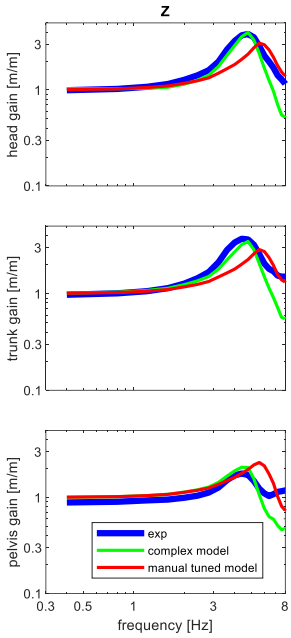

Figure A.3 Plots of vertiacal motion validation by manual tuning. Gains (upper 3 rows) and coherence (lower 3 rows) for head, trunk and pelvis in z displacement.

Appendix B. Nodes of grid search

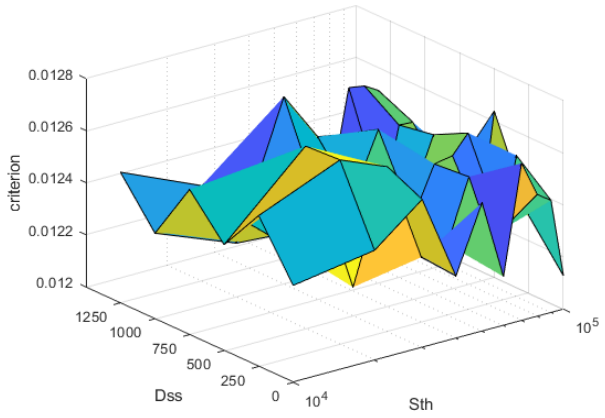

Figure B.1 Nodes of grid search and result surface plot of criterions for parameters Sth and Dss in vertical seat motion

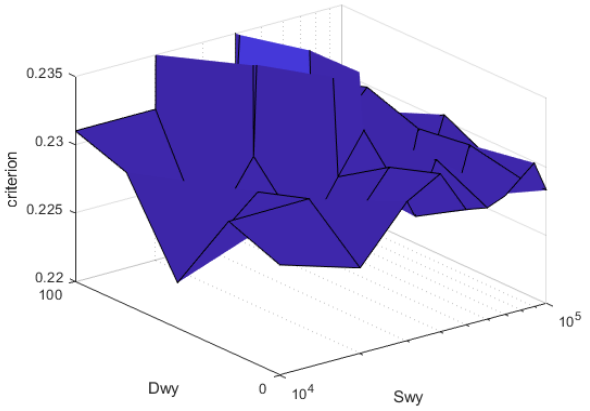

Figure B.2 Nodes of grid search and result surface plot of criterions for parameters Swy and Dwy in fore-aft seat motion

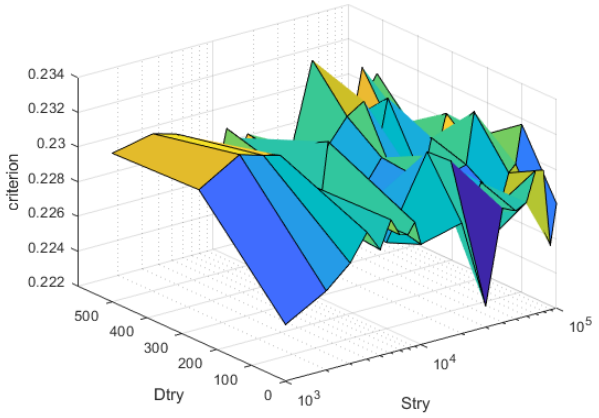

Figure B.3 Nodes of grid search and result surface plot of criterions for parameters Stry and Dtry in fore-aft seat motion

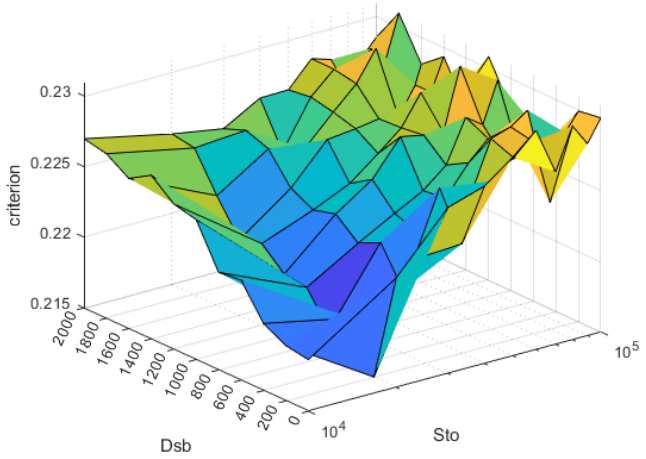

Figure B.4 Nodes of grid search and result surface plot of criterions for parameters Sto and Dsb in fore-aft seat motion

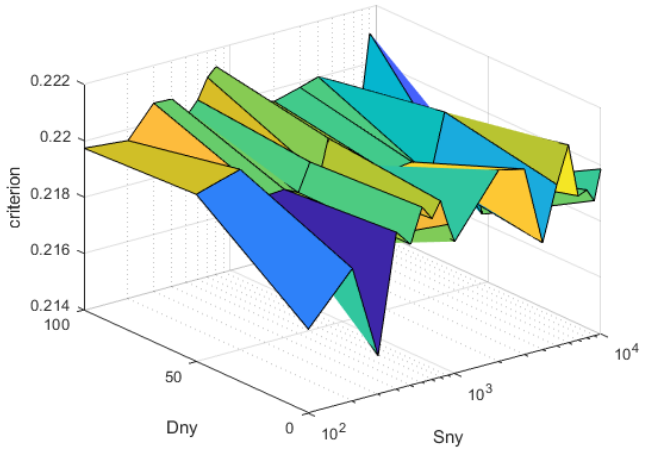

Figure B.5 Nodes of grid search and result surface plot of criterions for parameters Sny and Dny in fore-aft seat motion

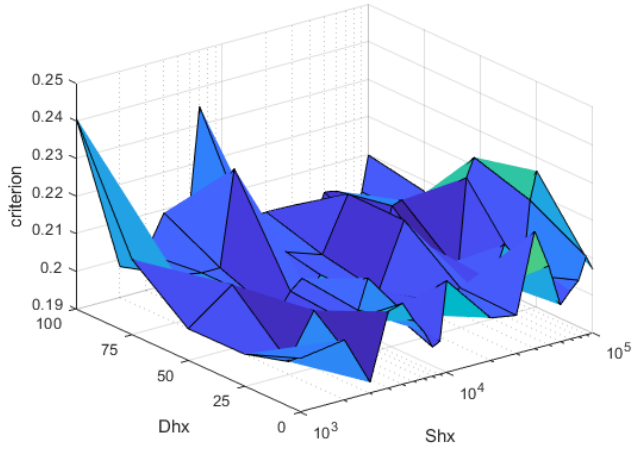

Figure B.6 Nodes of grid search and result surface plot of criterions for parameters Shx and Dhx in lateral seat motion

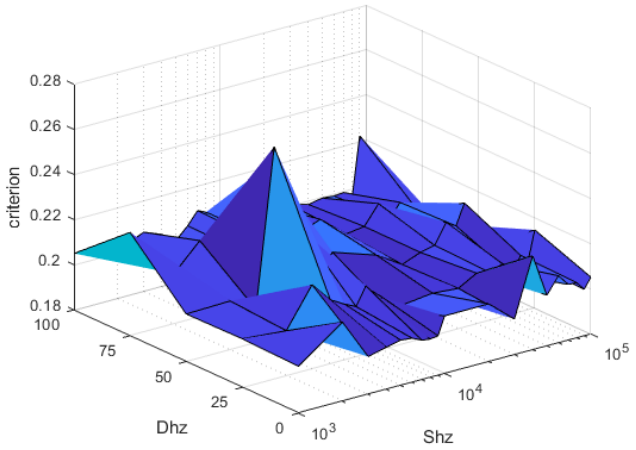

Figure B.7 Nodes of grid search and result surface plot of criterions for parameters Shz and Dhz in lateral seat motion

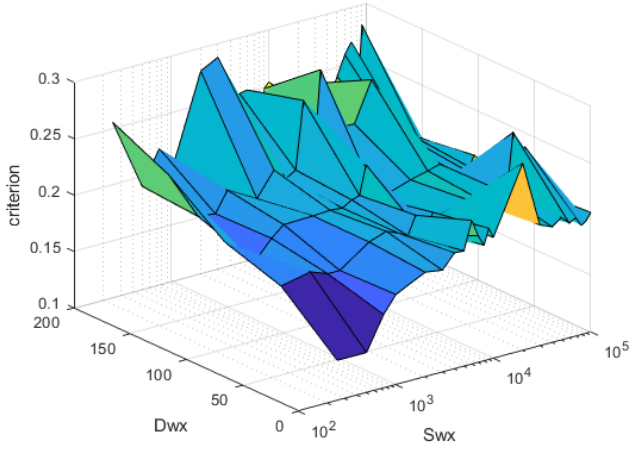

Figure B.8 Nodes of grid search and result surface plot of criterions for parameters Swx and Dwx in lateral seat motion

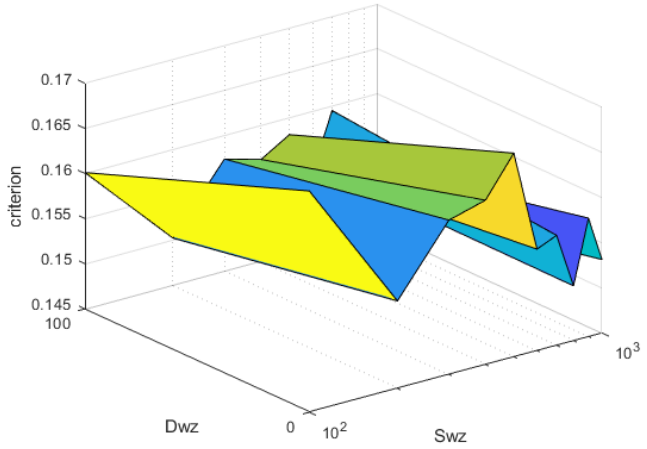

Figure B.9 Nodes of grid search and result surface plot of criterions for parameters Swz and Dwz in lateral seat motion

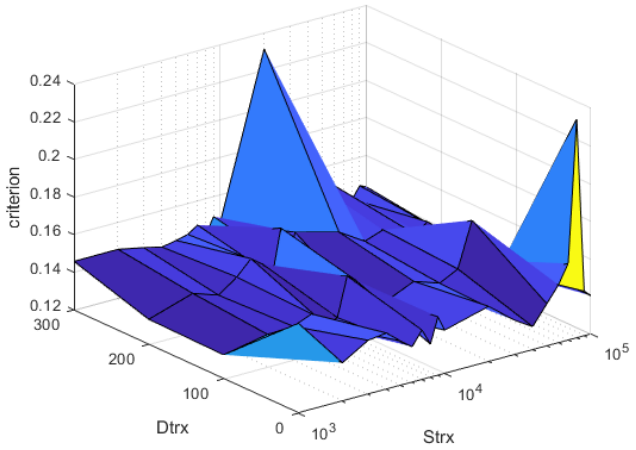

Figure B.10 Nodes of grid search and result surface plot of criterions for parameters Strx and Dtrx in lateral seat motion

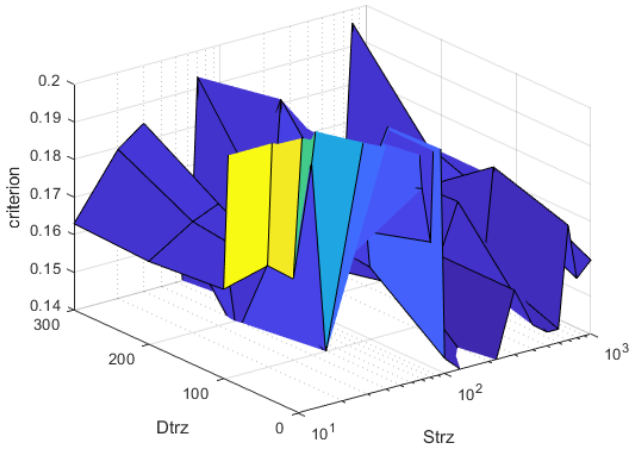

Figure B.11 Nodes of grid search and result surface plot of criterions for parameters Strz and Dtrz in lateral seat motion

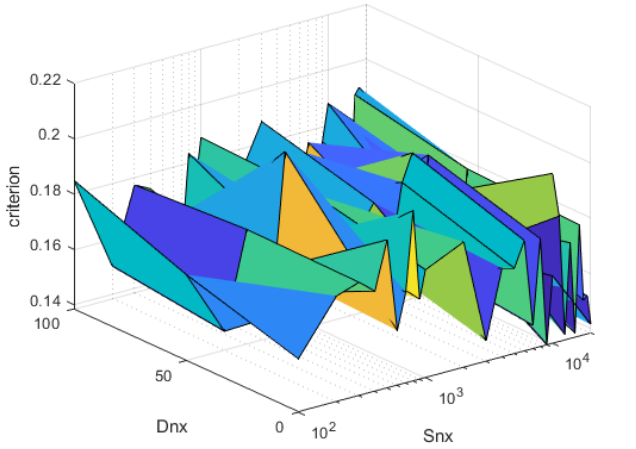

Figure B.12 Nodes of grid search and result surface plot of criterions for parameters Snx and Dnx in lateral seat motion

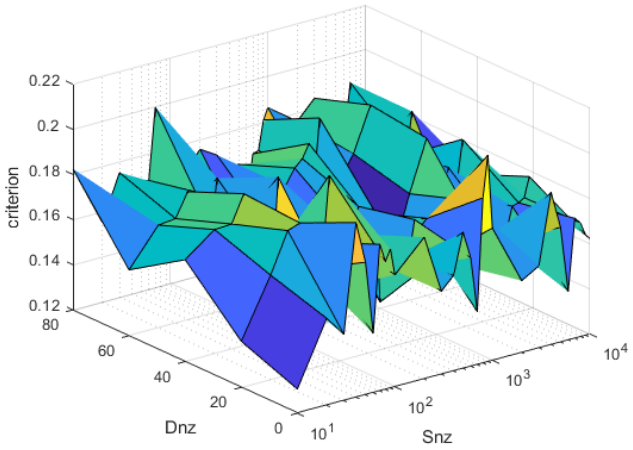

Figure B.13 Nodes of grid search and result surface plot of criterions for parameters Snz and Dnz in lateral seat motion

Appendix C. CPU time of SHM in lateral and vertical seat motion

Table C-1 CPU time of models in lateral seat motion

Subject	CPU(s)		
	SHM of time step = 1e-3s	SHM of time step = 5e-4s	SHM of time step = 2e-4s
Initialisation	0.1 (0%)	0.1 (0%)	0.0 (0%)
Element processing	0 (0%)	0 (0%)	0 (0%)
Element/Facet-Node/Vertex contact	0 (0%)	0 (0%)	0 (0%)
Multibody-Node/Vertex content	0 (0%)	0 (0%)	0 (0%)
Supports	0 (0%)	0 (0%)	0 (0%)
External loads	0 (0%)	0 (0%)	0 (0%)
Spowelds/FE rigid bodies/constraints	0 (0%)	0 (0%)	0 (0%)
FE time integration	0 (0%)	0 (0%)	0 (0%)
Total Finite Element	0 (0%)	0 (0%)	0 (0%)
Total Multi Body	140.0 (92%)	197.3 (91%)	328.3 (90%)
External program in coupling	6.1 (4%)	11.0 (5%)	24.0 (7%)
Output	3.8 (3%)	5.9 (3%)	10.4 (3%)
Filtering and injury	1.4 (1%)	1.6 (1%)	2.7 (1%)
Total	151.4 (100%)	215.9 (100%)	365.5 (100%)

Table C-2 CPU time of models in vertical seat motion

Subject	CPU(s)		
	SHM of time step = 1e-3s	SHM of time step = 5e-4s	SHM of time step = 2e-4s
Initialisation	0.1 (0%)	0.2 (0%)	0.1 (0%)
Element processing	0 (0%)	0 (0%)	0 (0%)
Element/Facet-Node/Vertex contact	0 (0%)	0 (0%)	0 (0%)
Multibody-Node/Vertex content	0 (0%)	0 (0%)	0 (0%)
Supports	0 (0%)	0 (0%)	0 (0%)
External loads	0 (0%)	0 (0%)	0 (0%)
Spowelds/FE rigid bodies/constraints	0 (0%)	0 (0%)	0 (0%)
FE time integration	0 (0%)	0 (0%)	0 (0%)
Total Finite Element	0 (0%)	0 (0%)	0 (0%)
Total Multi Body	140.8 (92%)	184.2 (91%)	321.9 (89%)
External program in coupling	6.2 (4%)	10.8 (5%)	2.6 (7%)
Output	4.3 (3%)	5.8 (3%)	10.2 (3%)
Filtering and injury	1.3 (1%)	1.6 (1%)	2.6 (1%)
Total	152.8 (100%)	202.5 (100%)	361.0 (100%)